Supporting information

Red-light photoswitching of indigos in polymer thin films

Kim Kuntze[a], Jani Viljakka[a], Matti Virkki[a], Chung-Yang (Dennis) Huang[b*], Stefan Hecht[c,d*] and Arri Priimagi[a*]

[a] Smart Photonic Materials, Faculty of Engineering and Natural Sciences, Tampere University, Fi-33101 Tampere, Finland. arri.priimagi@tuni.fi
[b] Institute for Chemical Reaction Design and Discovery (WPI-ICReDD), Hokkaido University, Kita 21, Nishi 10, Kita-ku, Sapporo, Hokkaido 001-0021, Japan.
[c] Department of Chemistry & IRIS Adlershof, Humboldt-Universität zu Berlin, Brook-Taylor-Strasse 2, 12489 Berlin, Germany.
[d] DWI – Leibniz Institute for Interactive Materials, Forckenbeckstrasse 50, 52074 Aachen, Germany.

Abstract

Through simple synthetic derivatisation, the parent indigo dye becomes a red-light *E*–*Z* photoswitch exhibiting negative photochromism and tuneable thermal isomerisation kinetics. These attributes make indigo derivatives extremely attractive for applications related to materials and living systems. However, there is a lack of knowledge in translating indigo photoswitching dynamics from solution to solid state – the environment crucial for most applications. Herein, we study the photoswitching performance of six structurally distinct indigo derivatives in five polymers of varying rigidity. Three key strategies are identified to enable efficient photoswitching under red (660 nm) light: (i) choosing a soft polymer matrix to minimise its resistance toward the isomerisation, (ii) creating free volume around the indigo molecules through synthetic modifications, and (iii) applying low dye loading (<1% w/w) to inhibit aggregation. These strategies are shown to improve both photostationary state distributions and the thermal stability of the *Z* isomer. When all three strategies are implemented, the isomerisation performance (>80% *Z* form in the photostationary state) is nearly identical to that in solution. These findings thus pave the way for designing new red-light photochromic materials based on indigos.

Table of contents

1. Supporting Results

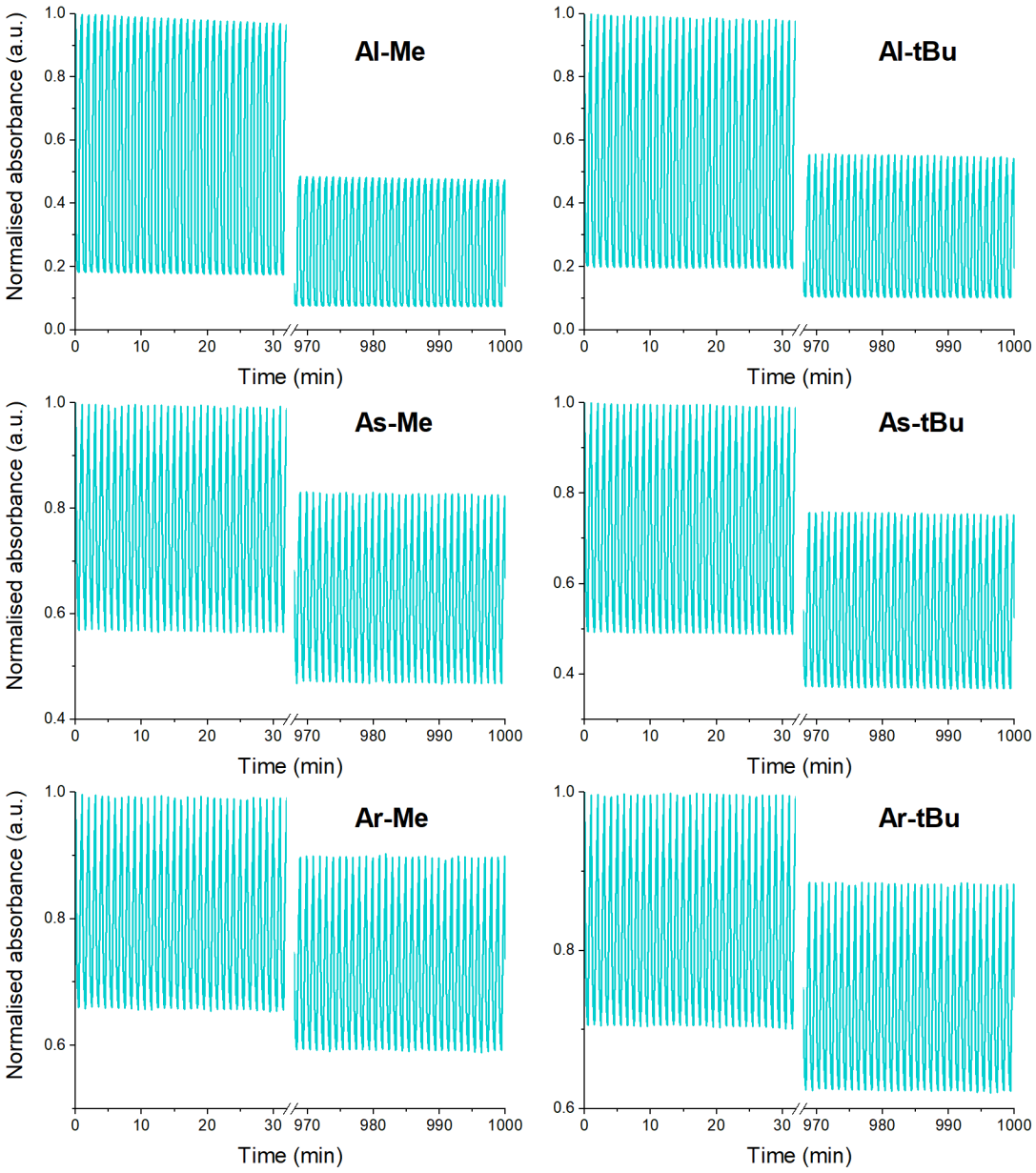

Figure S1*. 1,000 irradiation cycles (alternating 30 s pulses of 660 and 500 nm light) of the studied compounds in solution (50 µM in acetonitrile), showing that after 1,000 cycles 50–90 % of the initial dye concentration is conserved. The stability seems to be best for the aryl-substituted switches and worst for the alkyl-substituted switches.*

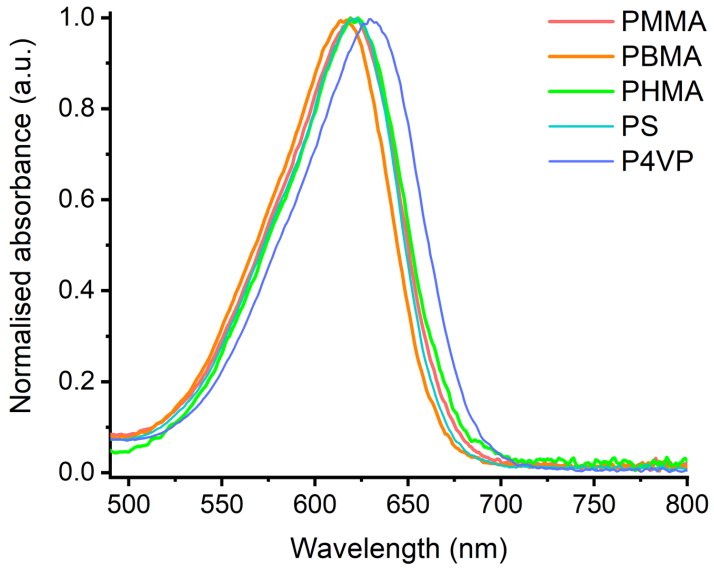

***Figure S2**. A zoom-in of the absorption spectrum of **Al-Me** in the studied polymer environments.*

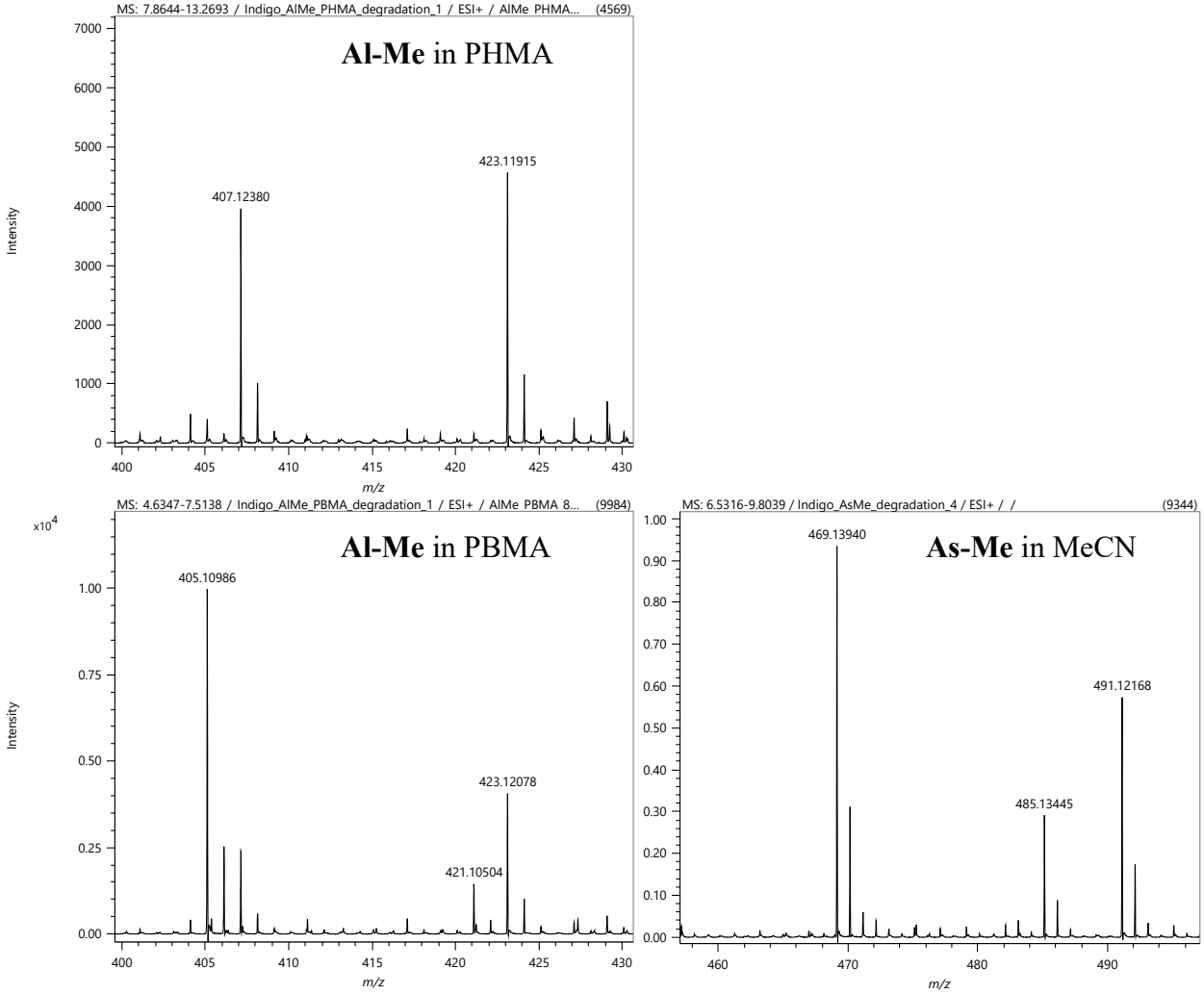

***Figure S3**. A zoom-in of the LC-MS spectra of degradation mixtures of **Al-Me** in PHMA and PBMA, and **As-Me** in MeCN. The spectra have been corrected to the $[M+H]^+$ signal, which for **Al-Me** is 407.1238 and for **As-Me** is 469.1394. In all three cases, a signal at $[M+16+H]^+$ is observed. In the case of Al-Me in PBMA, an additional signal at $[M–2+H]^+$ is visible at 405.10986.*

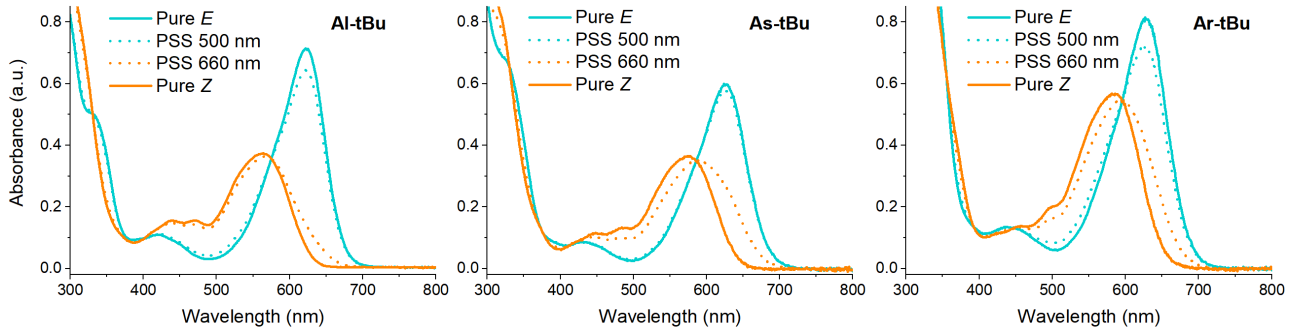

Figure S4. *Absorption spectra of the tert-butyl-substituted compounds in solution (50 µM in acetonitrile).*

Table S1. *Photochemical properties of the tert-butyl-substituted compounds in solution (50 µM in acetonitrile).*

	λ_E (nm)	λ_Z (nm)	$PSS_{660\ nm}$ (% *Z*)	$PSS_{500\ nm}$ (% *E*)	Dark (% *E*)	$t_{1/2}$ (min)
Al-tBu	623	564	87	89	100	2.5
As-tBu	626	576	68	95	100	3.9
Ar-tBu	627	584	73	84	82	26

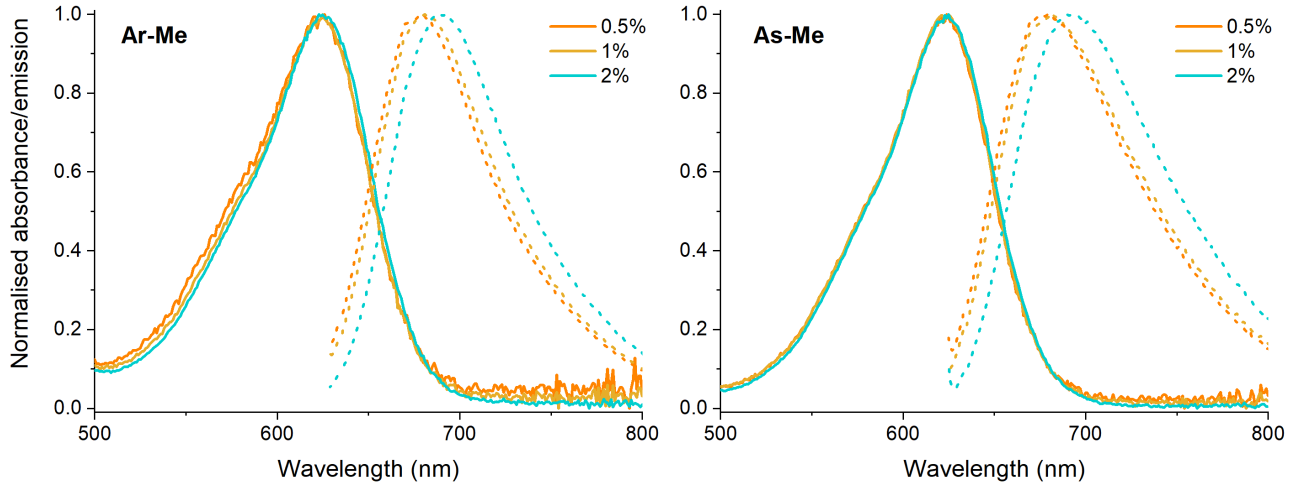

Figure S5. *A zoom-in of the absorption and fluorescence spectra of* ***Ar-Me and As-Me*** *(0.5–2%) in PHMA.*

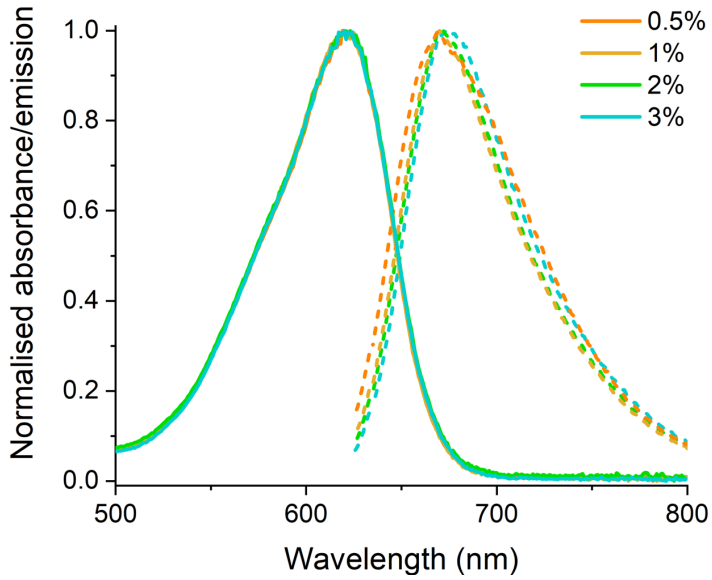

***Figure S6**. A zoom-in of the absorption and fluorescence spectra of **Al-Me** (0.5–3%) in PS.*

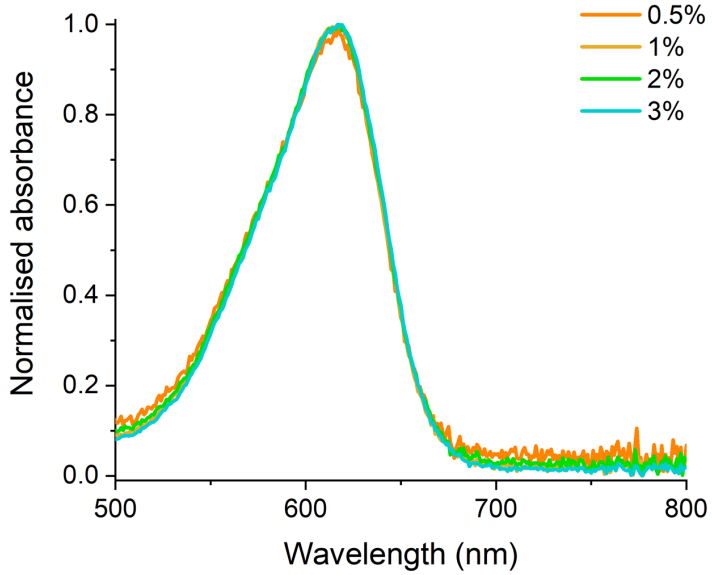

***Figure S7**. A zoom-in of the absorption spectrum of **Al-Me** (0.5–3%) in PBMA.*

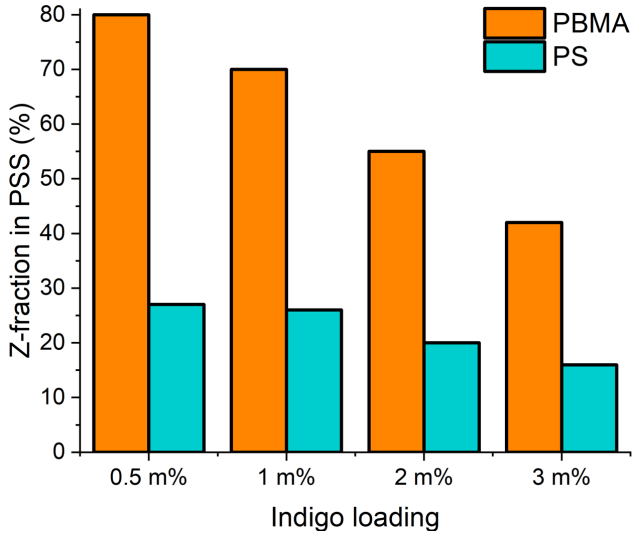

***Figure S8**. Z-fraction in PSS for **Al-Me** in PBMA and PS with different indigo loadings.*

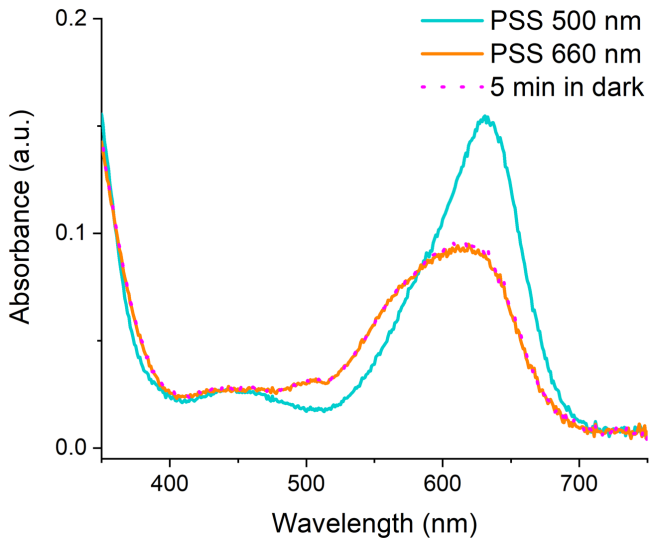

Figure S9. *Absorption spectrum of* ***Ar-tBu*** *in PS (0.5% w/w) upon irradiation with 500 nm and 660 nm light and 5 minutes after the 660 nm irradiation was stopped.*

***Table S2**. Compiled photochemical characteristics of studied indigo–polymer samples.*

Polymer	Indigo	w/w	Abs λ_{max}	Em λ_{max}	$PSS_{660\ nm}$ (% *Z*)	$t_{1/2}$ (min)
PHMA	Al-Me	0.25%	615	658	68	0.60
PHMA	Al-Me	0.5%	615	659	67	0.65
PHMA	Al-Me	1%	615	660	52	0.35
PHMA	Al-Me	2%	616	668	33	0.22
PHMA	Al-Me	3%	618	669	23	0.036
PHMA	Al-Me	5%	626	675	13	0.016
PHMA	Al-Me	10%	627	682	10	0.002
PHMA	Al-tBu	0.5%	621	665	83	4.55
PHMA	Al-tBu	1%	621	663	74	3.32
PHMA	Al-tBu	2%	621	663	57	1.68
PHMA	Al-tBu	3%	621	668	41	0.61
PHMA	Al-tBu	5%	621	671	26	0.32
PHMA	Al-tBu	10%	622	671	24	0.11
PHMA	Ar-Me	0.5%	625	680	68	-
PHMA	Ar-Me	1%	625	681	64	-
PHMA	Ar-Me	2%	625	692	40	-
PHMA	As-Me	0.5%	625	680	51	-
PHMA	As-Me	1%	625	682	43	-
PHMA	As-Me	2%	625	694	22	-
PHMA	Ar-tBu	0.5%	623	-	66	-
PHMA	Ar-tBu	1%	623	-	65	-
PHMA	Ar-tBu	2%	623	-	59	-
PHMA	As-tBu	0.5%	626	-	57	-
PHMA	As-tBu	1%	626	-	49	-
PHMA	As-tBu	2%	626	-	44	-
PBMA	Al-Me	0.5%	617	-	80	-
PBMA	Al-Me	1%	617	-	70	-
PBMA	Al-Me	2%	617	-	55	0.85
PBMA	Al-Me	3%	617	-	42	-
PBMA	Ar-Me	2%	626	-	47	101.8
PBMA	As-Me	2%	624	-	37	8.39
PMMA	Al-Me	2%	620	668	47	0.67
PMMA	Ar-Me	2%	628	686	19	21.97
PMMA	As-Me	2%	625	686	21	4.33
PS	Al-Me	0.5%	621	670	27	-
PS	Al-Me	1%	621	671	26	-
PS	Al-Me	2%	621	673	20	0.59
PS	Al-Me	3%	621	676	16	-
PS	Ar-Me	2%	626	696	16	29.37
PS	As-Me	2%	628	701	15	12.72
PS	Ar-tBu	0.5%	628	-	51	584.2
PS	Ar-tBu	1%	628	-	37	-
PS	Ar-tBu	2%	628	-	26	-
P4VP	Al-Me	2%	631	-	17	1.27
P4VP	Ar-Me	2%	635	-	18	10.9[a]
P4VP	As-Me	2%	635	-	12	8.89

[a] Due to large stretched exponential fitting error margins, a biexponential fit was used instead (see p. S28–S29 and S31).

2. Experimental details

Synthesis

Synthetic work was carried out in Tampere University. All reagents, polymers and solvents were commercial and purchased from Sigma Aldrich, TCI Europe, VWR, PolymerSource or FluoroChem. When needed, dry solvents were acquired using an Inert PureSolv solvent purification system. Reactions were monitored with thin-layer chromatography (TLC) on commercial Merck Silica 60 F_{254} TLC plates, and the developed plates were visualized with UV irradiation (254 nm) or with a potassium permanganate stain.

Accurate mass experiments were performed with the JEOL JMS-T100LP AccuTOF LC-plus 4G Time-of-Flight mass spectrometer using electrospray ionization. Nuclear magnetic resonance spectra (NMR) were measured with a 500 MHz JEOL ECZR 500 (125 MHz for ^{13}C) at 25 °C and processed with the JEOL Delta NMR software version 5.3.1 (Windows). Chemical shifts are given in ppm and are referenced to solvent signals ($CHCl_3$: δ = 7.26 ppm (^1H), 77.16 ppm (^{13}C). Multiplicities are abbreviated as follows: singlet (s), doublet (d), triplet (t), quartet (q), pentet (p), and multiplet (m). Coupling constants (*J*) are given in Hz.

Al-Me: Dimethyl 4,4'-(3,3'-dioxo-[2,2'-biindolinylidene]-1,1'-diyl)(*E*)-dibenzoate

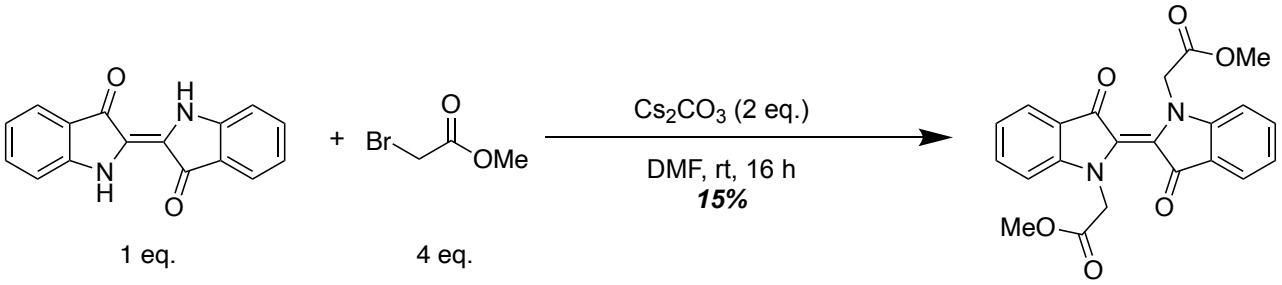

Indigo (2.0 g, 7.7 mmol), methyl bromoacetate (2.84 ml, 30.8 mmol) and caesium carbonate (5.0 g, 15.4 mmol) were stirred in *N*,*N*-dimethylformamide (50 ml) at room temperature overnight. The reaction mixture was then filtered through a plug of SiO_2, diluted with ethyl acetate, washed with brine and three times with water, dried with magnesium sulphate, concentrated and purified by flash column chromatography (SiO_2, 40% ethyl acetate in hexane) to yield **Al-Me** (380 mg, 15%) as a turquoise solid. ^1H-NMR (500 MHz, $CDCl_3$) δ 7.72 (d, J = 6.9 Hz, 2H), 7.52 (t, J = 7.2 Hz, 2H), 7.06 (t, J = 7.4 Hz, 2H), 7.00 (d, J = 8.0 Hz, 2H), 4.81 (s, 4H), 3.75 (s, 6H). ^{13}C-NMR (126 MHz, $CDCl_3$) δ 186.3, 169.5, 153.7, 135.8, 127.0, 124.5, 122.1, 122.0, 111.1, 52.5, 50.9. HRMS (ESI+): *m/z* calcd. for $[C_{22}H_{18}N_2O_6+Na^+]$: 429.10571; found: 429.10521.

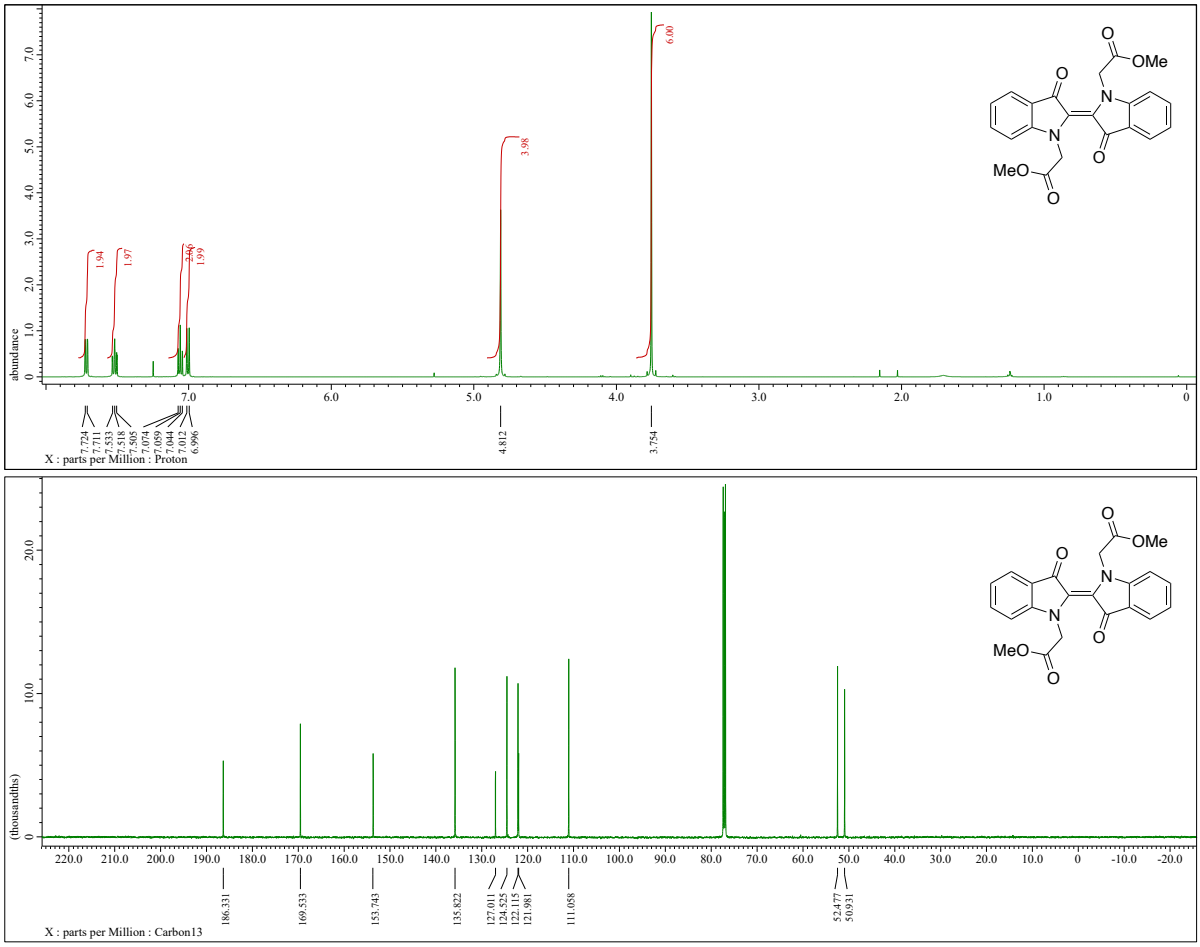

Ar-Me: Dimethyl 4,4'-(3,3'-dioxo-[2,2'-biindolinylidene]-1,1'-diyl)(*E*)-dibenzoate

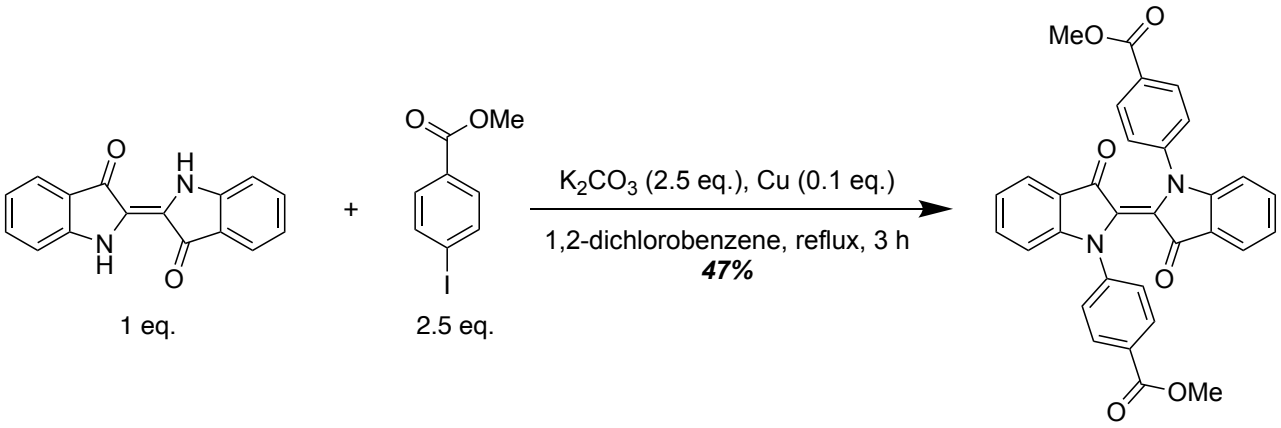

Indigo (400 mg, 1.53 mmol), methyl 4-iodobenzoate (1.05 g, 3.82 mmol) and copper powder (10 mg, 153 µmol) were refluxed in bubble-degassed dichlorobenzene (20 ml) under argon for 3 hours. The appearance of a deep blue monoarylated indigo was first observed, followed by its disappearance and the appearance of a turquoise diarylated trans product, isomerizing to the purple cis isomer in the mixture. The crude product was filtered through a plug of SiO_2, concentrated and purified by column (SiO_2, from pure dichloromethane to 20% ethyl acetate in dichloromethane) to yield the product (365 mg, 47%) as a turquoise solid. ^{1}H-NMR (500 MHz, $CDCl_3$) δ 8.20 (d, J = 8.6 Hz, 4H), 7.60 (d, J = 8.6 Hz, 4H), 7.54 (d, J = 7.4 Hz, 2H), 7.38 (t, J = 8.0 Hz, 2H), 7.06 (d, J = 8.6 Hz, 2H), 7.00 (t, J = 7.4 Hz, 2H), 3.91 (s, 6H). ^{13}C-NMR (126 MHz, $CDCl_3$) δ 184.2, 166.3, 152.5, 146.0, 135.4, 131.2, 128.5, 126.1, 125.4, 124.5, 122.7, 121.8, 111.2, 52.4. HRMS (ESI+): *m/z* calcd. for

[$C_{32}H_{22}N_2O_6$+Na^+]: 553.13701; found: 553.13711. Note: the unassigned low-intensity peaks belong to the *Z* isomer that is present in a thermodynamic equilibrium.

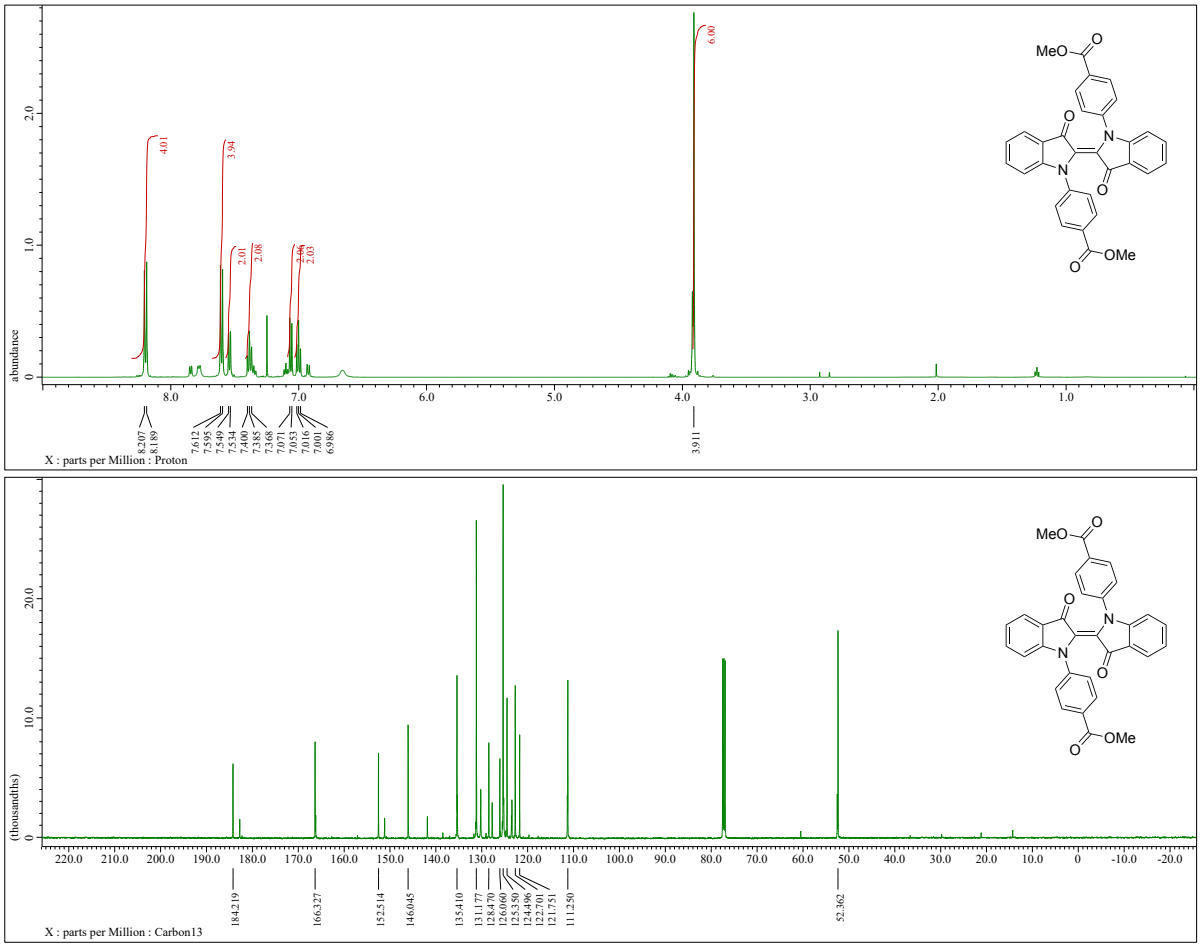

As-Me-pre: Methyl (*E*)-4-(3,3'-dioxo-[2,2'-biindolinylidene]-1-yl)benzoate

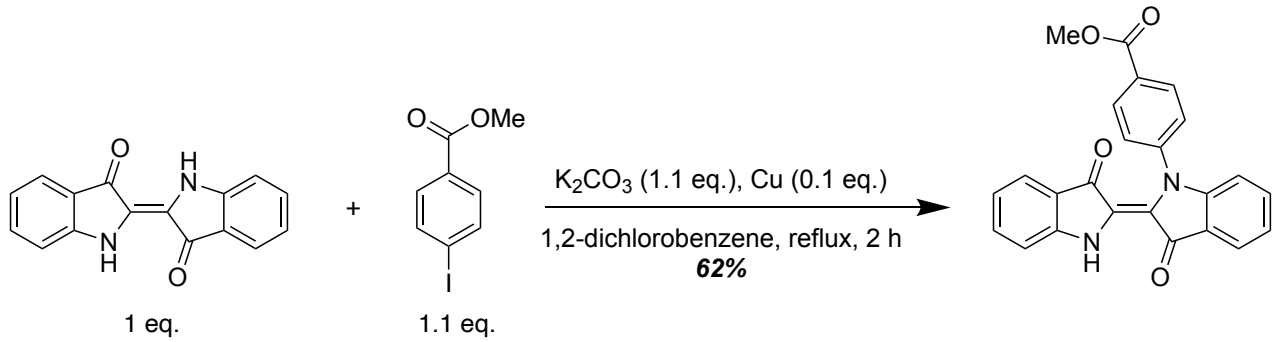

Indigo (200 mg, 0.77 mmol), methyl 4-iodobenzoate (233 mg, 0.85 mmol), potassium carbonate (117 mg, 0.85 mmol) and copper powder (5 mg, 0.077 mmol) were refluxed in bubble-degassed 1,2-dichlorobenzene (8 ml) under an argon atmosphere for 1.5 hours. The reaction mixture was filtered through a plug of SiO_2, concentrated and purified by flash column chromatography (SiO_2, pure dichloromethane to 10% ethyl acetate in dichloromethane) to yield **As-Me-pre** (189 mg, 62%) as a dark blue solid. ^{1}H-NMR (500 MHz, $CDCl_3$) δ 10.47 (s, 1H), 8.17 (d, J = 8.0 Hz, 2H), 7.82 (d, J = 7.4 Hz, 1H), 7.46 (t, J = 7.2 Hz, 2H), 7.43-7.40 (m, 3H), 7.09 (t, J = 7.4 Hz, 1H), 7.00 (t, J = 8.6 Hz, 2H), 6.89 (t, J = 7.4 Hz, 1H), 3.93 (s, 3H). ^{13}C-NMR (126 MHz, $CDCl_3$) δ 189.5, 185.8, 166.5, 153.1,

151.5, 144.8, 136.2, 135.8, 130.8, 128.7, 126.2, 126.1, 124.9, 124.1, 122.0, 121.3, 121.2, 121.1, 120.1, 112.0, 111.6, 52.3. HRMS (ESI+): *m/z* calcd. for [$C_{24}H_{16}N_2O_4$+Na^+]: 419.10023; found: 419.09995.

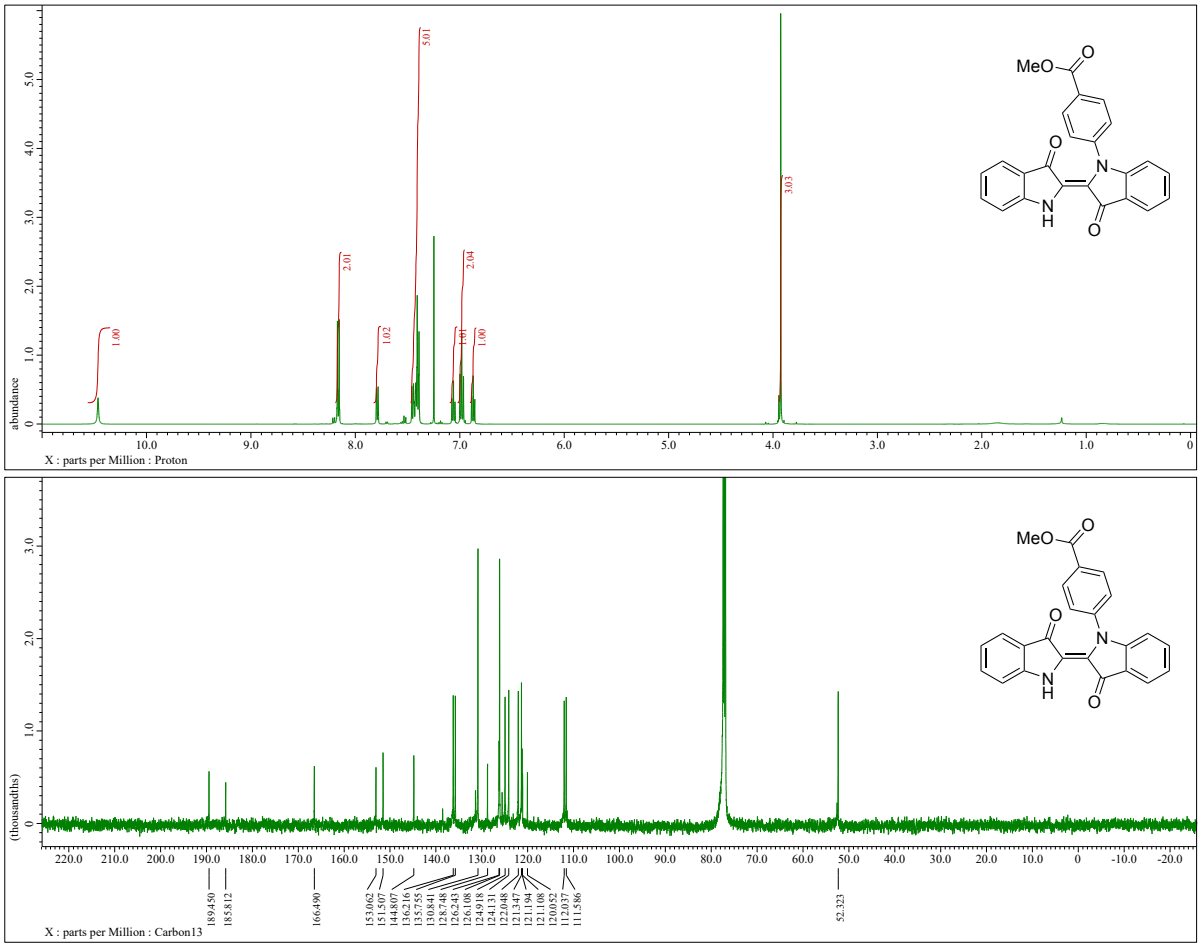

As-Me: Methyl (*E*)-4-(1'-(2-methoxy-2-oxoethyl)-3,3'-dioxo-[2,2'-biindolinylidene]-1-yl)benzoate

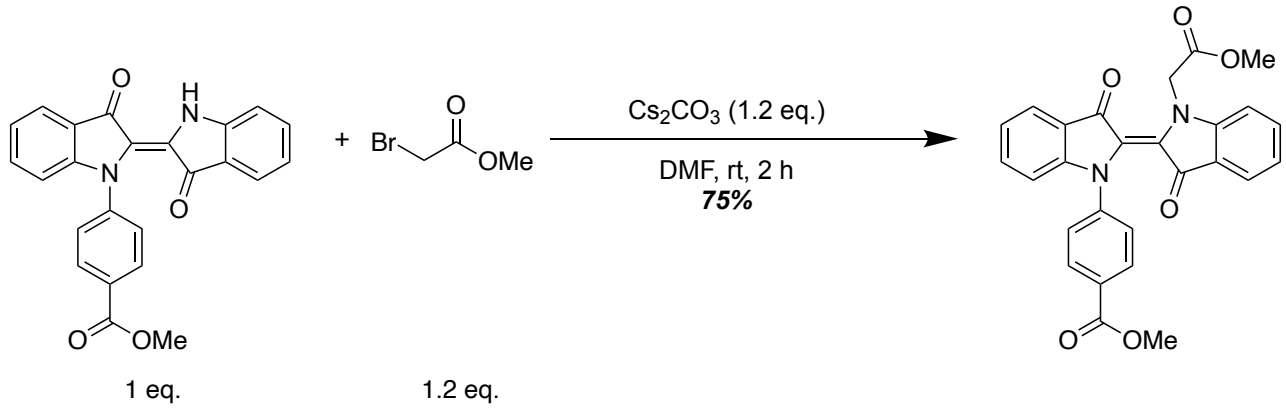

As-Me-pre (49.4 mg, 0.134 mmol), methyl bromoacetate (14.9 µl, 0.161 mmol) and caesium carbonate (52.5 mg, 0.161 mmol) were stirred in *N*,*N*-dimethylformamide (2 ml) at room temperature for 2 hours. The reaction mixture was then diluted with ethyl acetate, washed with brine and three times with water, dried with magnesium sulphate, concentrated and purified by flash column chromatography (pure dichloromethane to 5% ethyl acetate in dichloromethane) to yield **As-Me** (44.1 mg, 75%) as a turquoise solid. ^{1}H-NMR (500 MHz, $CDCl_3$) δ 8.14 (d, J = 8.6 Hz, 2H), 7.79 (d, J =

6.9 Hz, 1H), 7.57 (d, J = 8.6 Hz, 2H), 7.42-7.52 (m, 3H), 7.18 (d, J = 8.6 Hz, 1H), 7.09 (t, J = 7.4 Hz, 1H), 6.99 (s, 2H), 5.20 (s, 2H), 3.89 (s, 3H), 3.77 (s, 3H). ^{13}C-NMR (126 MHz, $CDCl_3$) δ 186.0, 184.4, 169.2, 166.5, 153.0, 152.4, 146.3, 135.7, 135.4, 131.0, 129.2, 127.9, 125.1, 124.7, 124.5, 124.1, 122.5, 122.4, 122.2, 121.9, 111.3, 110.5, 52.7, 52.3, 49.9. HRMS (ESI+): *m/z* calcd. for [$C_{27}H_{20}N_2O_6$+Na^+]: 491.12136; found: 491.11888.

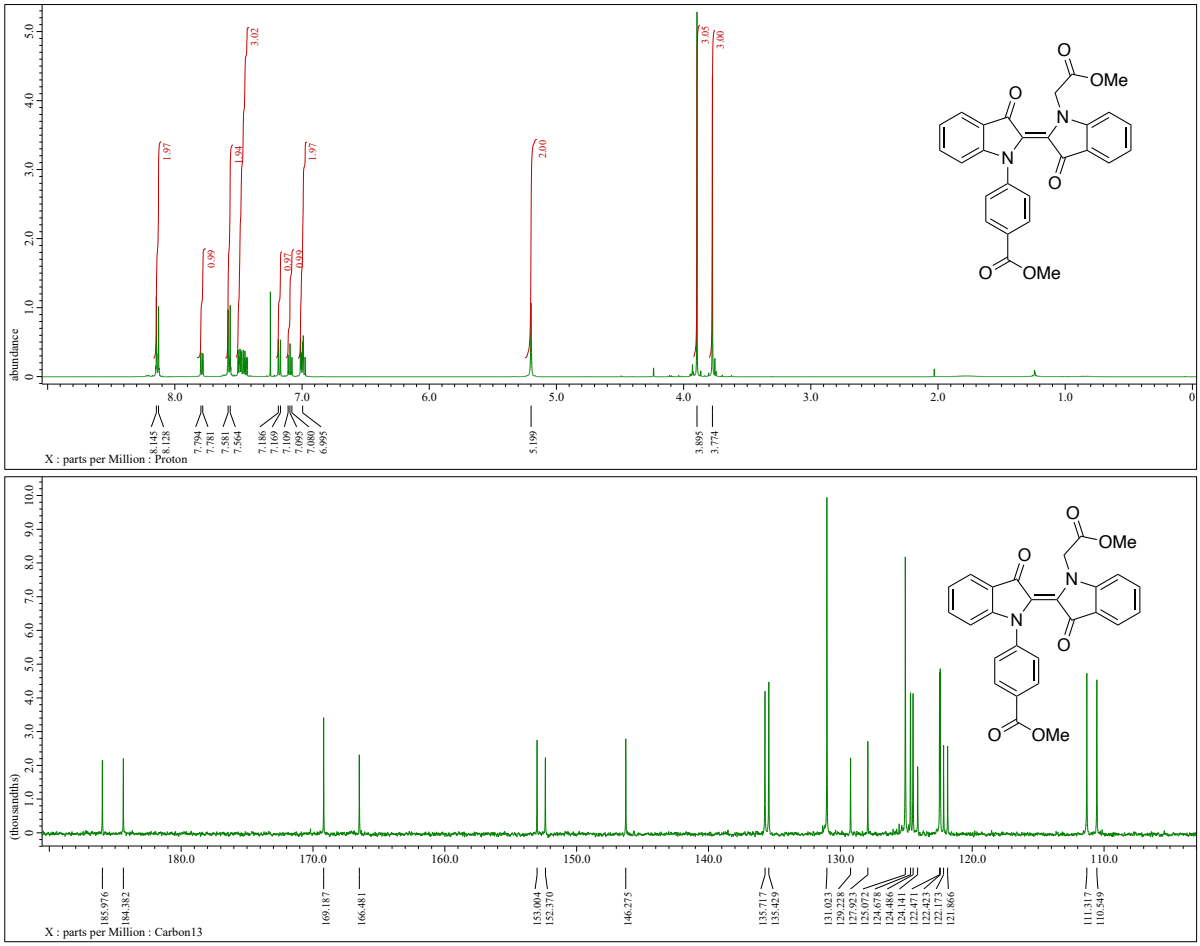

Al-tBu: Di-*tert*-butyl 2,2'-(3,3'-dioxo-[2,2'-biindolinylidene]-1,1'-diyl)(*E*)-diacetate

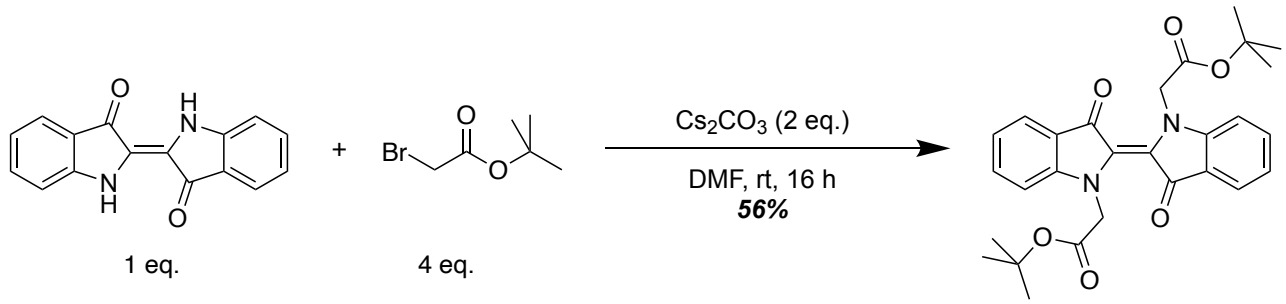

Indigo (1.0 g, 3.85 mmol), *tert*-butyl bromoacetate (2.26 ml, 15.4 mmol) and caesium carbonate (2.5 g, 7.7 mmol) were stirred in *N*,*N*-dimethylformamide (10 ml) at room temperature overnight. The reaction mixture was filtered through a plug of SiO_2, diluted with ethyl acetate, washed twice with brine and twice with water, dried with magnesium sulphate, concentrated and purified by flash column chromatography (pure hexane to 30% ethyl acetate in hexane) to yield **Al-tBu** (810 mg, 56%) as a turquoise solid. ^{1}H-NMR (500 MHz, $CDCl_3$) δ 7.72 (d, J = 7.4 Hz, 2H), 7.51 (t, J = 7.7 Hz, 2H), 7.05 (t, J = 7.2 Hz, 2H), 7.00 (d, J = 8.0 Hz, 2H), 4.73 (s, 4H), 1.38 (s, 18H). ^{13}C-NMR (126 MHz,

$CDCl_3$) δ 186.3, 167.8, 153.8, 135.6, 127.3, 124.4, 122.1, 121.8, 111.0, 82.3, 51.8, 28.1. HRMS (ESI+): *m/z* calcd. for [$C_{28}H_{30}N_2O_6$+Na^+]: 513.19961; found: 513.19771.

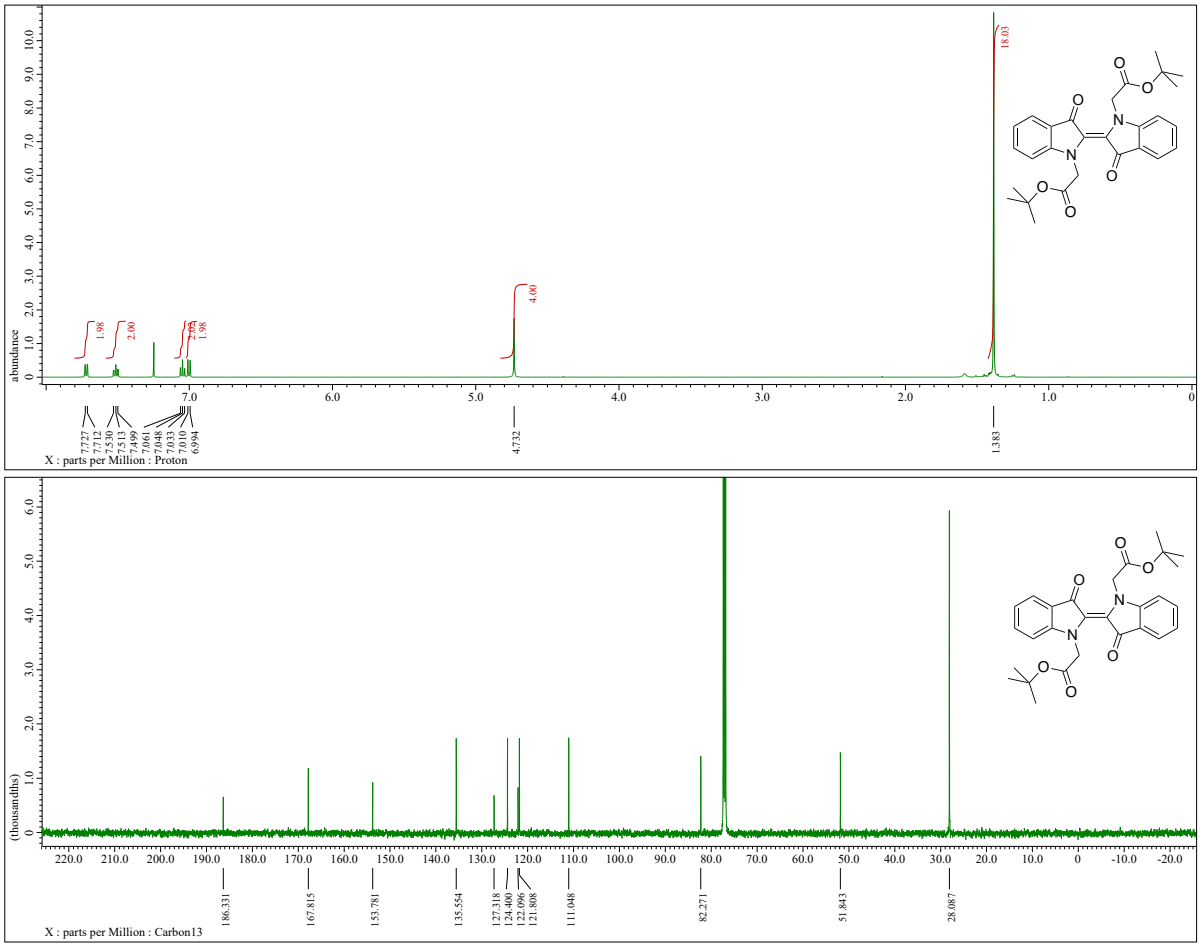

Tert-butyl 4-iodobenzoate

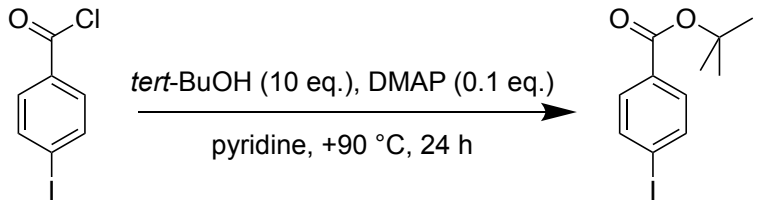

1 eq.

Prepared according to a patent [2]. ^{1}H-NMR (500 MHz, $CDCl_3$) δ 7.75 (d, J = 8.6 Hz, 2H), 7.67 (d, J = 8.6 Hz, 2H), 1.57 (s, 9H).

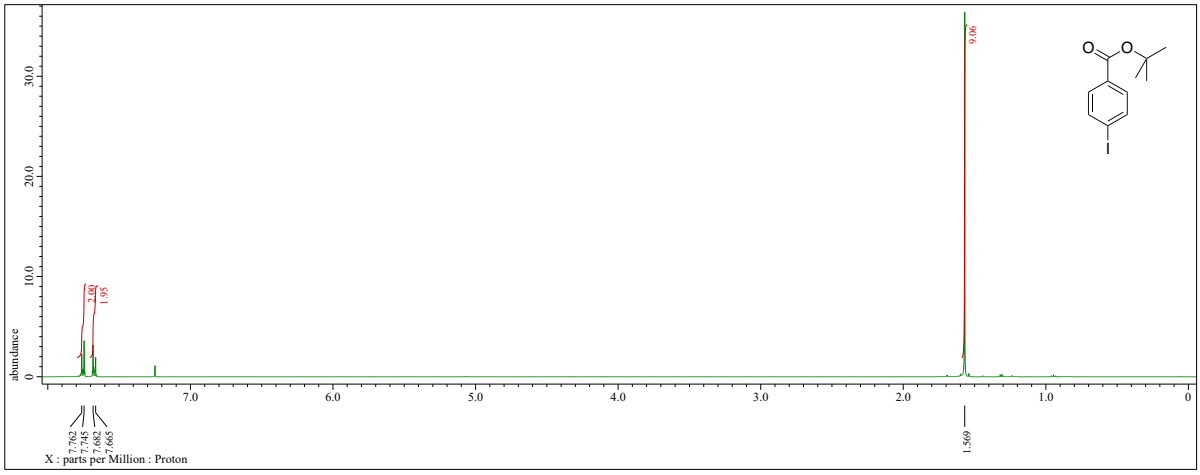

Ar-tBu and As-tBu-pre: di-tert-butyl 4,4'-(3,3'-dioxo-[2,2'-biindolinylidene]-1,1'-diyl)(E)-dibenzoate and tert-butyl (E)-4-(3,3'-dioxo-[2,2'-biindolinylidene]-1-yl)benzoate

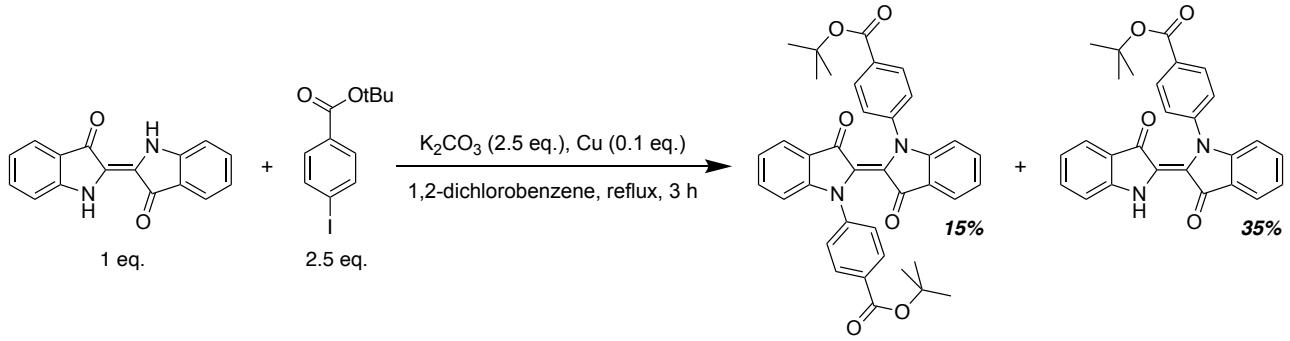

Indigo (309 mg, 1.19 mmol), *tert*-butyl 4-iodobenzoate (566 mg, 1.78 mmol), potassium carbonate (328 mg, 2.38 mmol) and copper powder (7.6 mg, 0.12 mmol) were refluxed in bubble-degassed 1,2-dichlorobenzene (10 ml) under argon for 5 hours. The reaction mixture was then allowed to cool down, filtered through a plug of SiO_2 and purified by flash column chromatography (SiO_2, 0–10% ethyl acetate in dichloromethane) to yield **Ar-tBu** (98 mg, 15%) and **As-tBu-pre** (181 mg, 35%) as turquoise-blue and deep blue solids. **Ar-tBu**: ^{1}H-NMR (500 MHz, $CDCl_3$) δ 8.17 (d, J = 8.6 Hz, 4H), 7.59 (d, J = 8.0 Hz, 6H), 7.40 (t, J = 7.7 Hz, 2H), 7.07 (d, J = 8.6 Hz, 2H), 7.02 (t, J = 7.4 Hz, 2H), 1.60 (s, 18H). ^{13}C-NMR (126 MHz, $CDCl_3$) δ 184.4, 165.0, 152.7, 145.6, 135.3, 131.0, 130.4, 126.3, 125.2, 124.5, 122.7, 121.8, 111.3, 81.4, 28.3. HRMS (ESI+): *m/z* calcd. for [$C_{38}H_{34}N_2O_6$+Na^+]: 637.23091; found: 637.23370. Note: the unassigned low-intensity peaks belong to the *Z* isomer that is present in a thermodynamic equilibrium. **As-tBu-pre**: ^{1}H-NMR (500 MHz, $CDCl_3$) δ 10.47 (s, 1H), 8.12 (d, J = 8.6 Hz, 2H), 7.81 (d, J = 7.4 Hz, 1H), 7.48 (d, J = 7.4 Hz, 1H), 7.42 (t, J = 7.7 Hz, 2H), 7.38 (d, J = 8.6 Hz, 2H), 7.07 (t, J = 7.2 Hz, 1H), 6.98 (q, J = 4.0 Hz, 2H), 6.88 (t, J = 7.4 Hz, 1H), 1.61 (s, 9H). ^{13}C-NMR (126 MHz, $CDCl_3$) δ 189.5, 185.9, 165.1, 153.2, 151.5, 144.3, 136.2, 135.7, 130.7, 126.2, 125.9, 124.9, 124.1, 122.0, 121.3, 121.2, 121.1, 120.1, 112.0, 111.6, 81.3, 28.3. HRMS (ESI+): *m/z* calcd. for [$C_{27}H_{22}N_2O_4$+Na^+]: 461.14718; found: 461.14655.

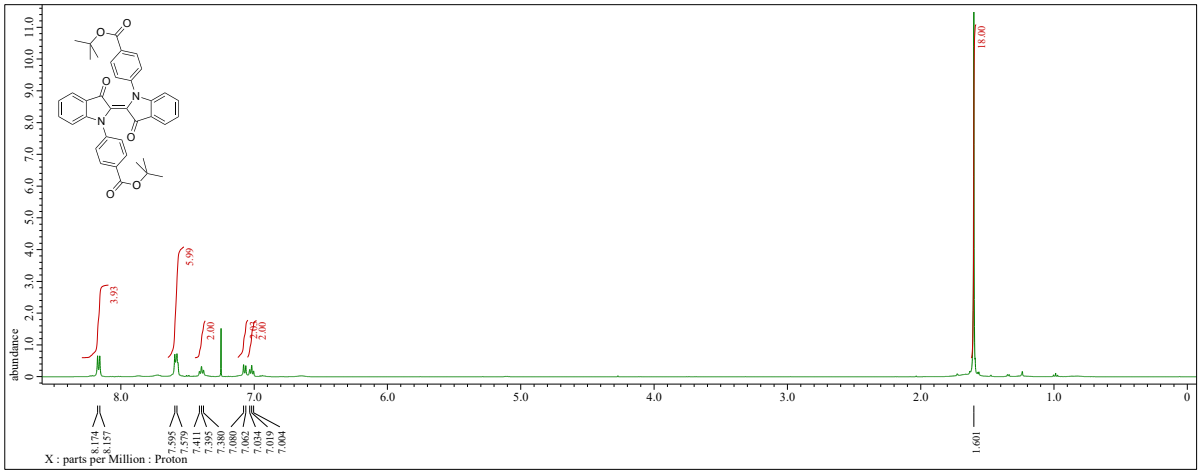
abundance
3.93
5.99
2.00
2.03
2.00
18.00
8.174
8.157
7.595
7.579
7.411
7.395
7.380
7.080
7.062
7.034
7.019
7.004
1.601
X : parts per Million : Proton

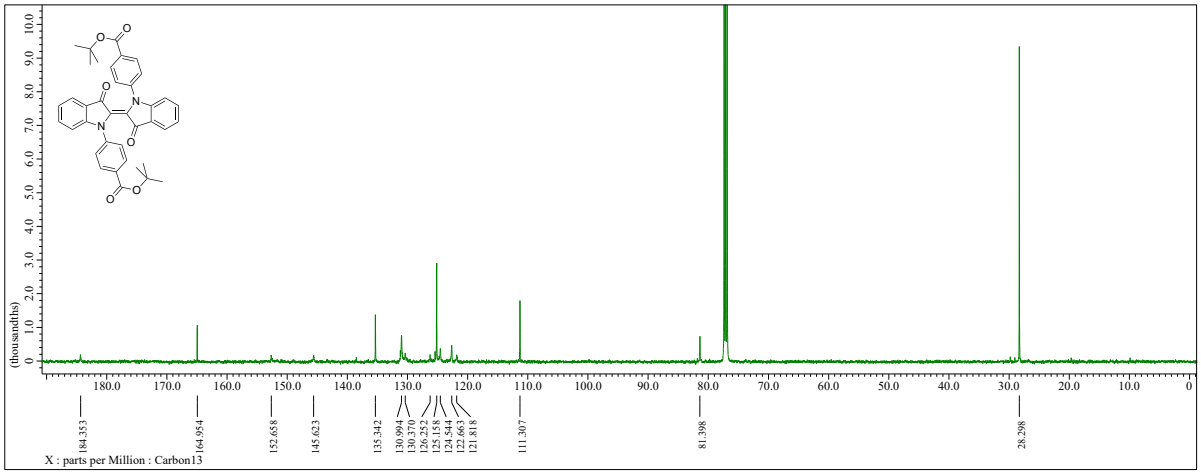
(thousandths)
184.353
164.954
152.658
145.623
135.342
130.994
130.370
128.253
125.158
124.544
122.663
121.818
111.307
81.398
28.298
X : parts per Million : Carbon13

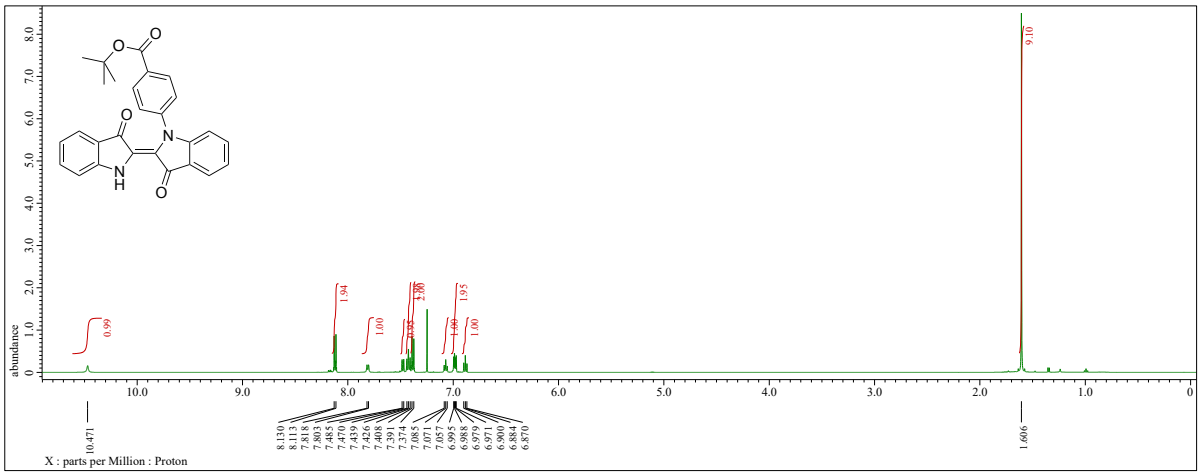
abundance
0.99
1.94
1.00
1.95
1.00
9.10
10.471
8.130
8.113
7.818
7.803
7.485
7.470
7.410
7.426
7.408
7.391
7.374
7.085
7.071
7.057
6.995
6.988
6.979
6.971
6.900
6.884
6.870
1.606
X : parts per Million : Proton

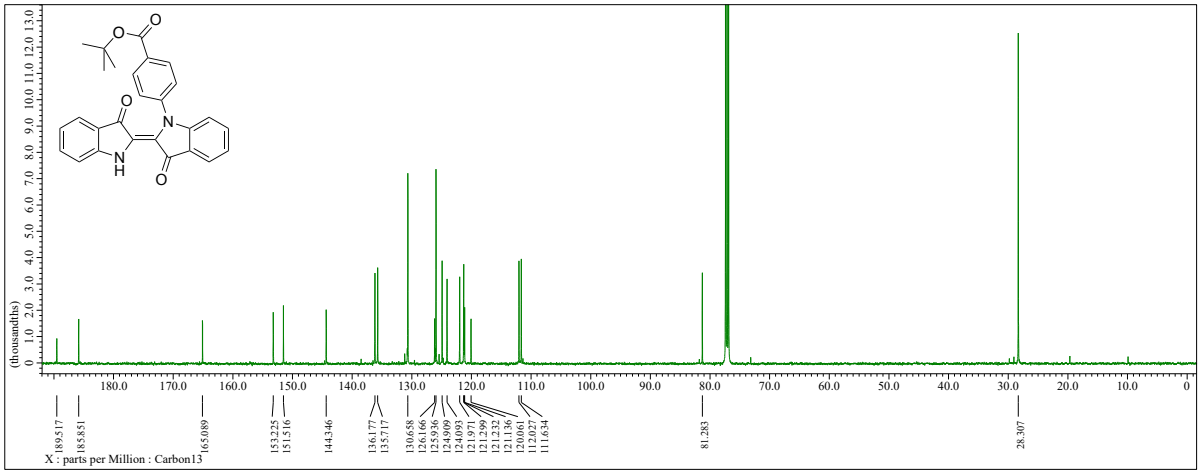

As-tBu: tert-butyl (E)-4-(1'-(2-(tert-butoxy)-2-oxoethyl)-3,3'-dioxo-[2,2'-biindolinylidene]-1-yl)benzoate

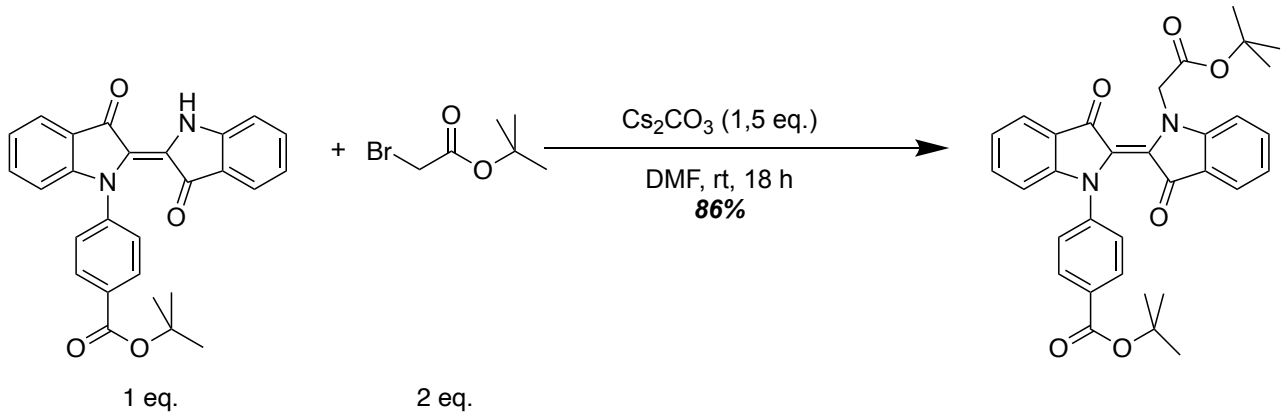

As-tBu-pre (148 mg, 0.34 mmol), tert-butyl bromoacetate (100 µl, 0.68 mmol) and caesium carbonate (133 mg, 0.41 mmol) were stirred in dry *N*,*N*-dimethylformamide (3 ml) overnight. The reaction mixture was then diluted with ethyl acetate, washed with brine, three times with water and again with brine, dried with magnesium sulphate, concentrated and purified by flash column chromatography (SiO_2, 0–10% ethyl acetate in dichloromethane) to yield **As-tBu** (160 mg, 86%) as a turquoise-blue solid. ^{1}H-NMR (500 MHz, $CDCl_3$) δ 8.08 (d, J = 8.6 Hz, 2H), 7.79 (d, J = 7.4 Hz, 1H), 7.55-7.42 (m, 5H), 7.18 (d, J = 8.0 Hz, 1H), 7.09 (t, J = 7.4 Hz, 1H), 6.99 (q, J = 8.2 Hz, 2H), 5.07 (s, 2H), 1.58 (s, 9H), 1.40 (s, 9H). ^{13}C-NMR (126 MHz, $CDCl_3$) δ 185.8, 184.7, 167.7, 165.1, 153.4, 152.4, 145.9, 135.6, 135.3, 130.8, 129.8, 129.5, 124.8, 124.6, 124.4, 124.2, 122.3, 122.2, 121.9, 111.3, 110.6, 82.8, 81.2, 51.0, 28.3, 28.1. HRMS (ESI+): *m/z* calcd. for [$C_{33}H_{32}N_2O_6$+Na^+]: 575.21526; found: 575.21450.

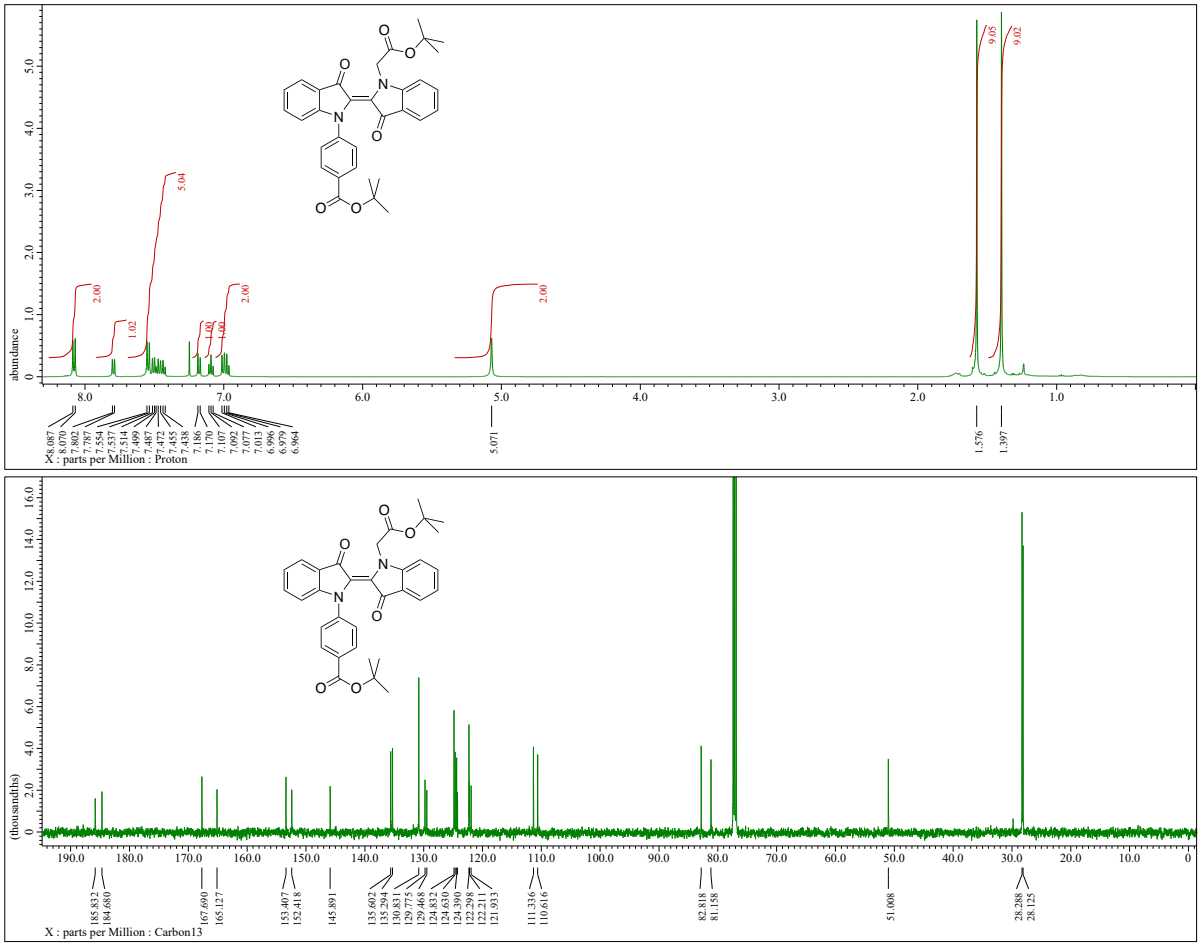

Photochemical characterisation

UV-visible absorption spectra were recorded with an Agilent Cary 60 spectrophotometer equipped with an Ocean Optics Qpod 2e Peltier-thermostated cell holder whose temperature accuracy is 0.1 °C. Photoexcitation was conducted using a Prior Lumen 1600 light source containing multiple narrow-band LEDs at different wavelengths. The illumination intensities were acquired by measuring the illumination powers with a Coherent LabMax thermal power meter and dividing the number by the area of the cuvette (0.78 cm^{-2}) or polymer film (0.38 cm^{-2}) being illuminated. Quartz fluorescence cuvettes with an optical path of 1.0 cm were used for all measurements. Molar absorption coefficients were calculated with the Beer-Lambert law.

Photostationary state (PSS) refers to the mixture of isomers upon constant illumination with a chosen excitation wavelength. Dark, in turn, refers to the mixture of isomers after an elongated period in a dark cavity at room temperature or in an elevated temperature. Based on the thermal relaxation lifetime of the molecules, the time and temperature were chosen so that the dark mixture would consist of molecules only in the *E* state, with the exception of **Ar-Me** that reached an equilibrium with 78% *E* in dark.

Generally, the PSS compositions were determined from the UV-visible spectra by comparing the absorbance values of the pure *E* spectrum and the PSS spectrum in the red end of the *E* isomer absorption band where the *Z* isomer does not absorb, following a previously published method [1]. For **Ar-Me** and **Ar-tBu** the compositions in solution were determined with ^{1}H NMR spectroscopy by comparing the integrals of two isolated (not overlapping) aromatic two-proton signals originating

from the *E* and *Z* isomers (**Fig. S10**). The photochemical parameters for each compound are presented in **Table 1** in the manuscript and **Table S1** (*vide supra*).

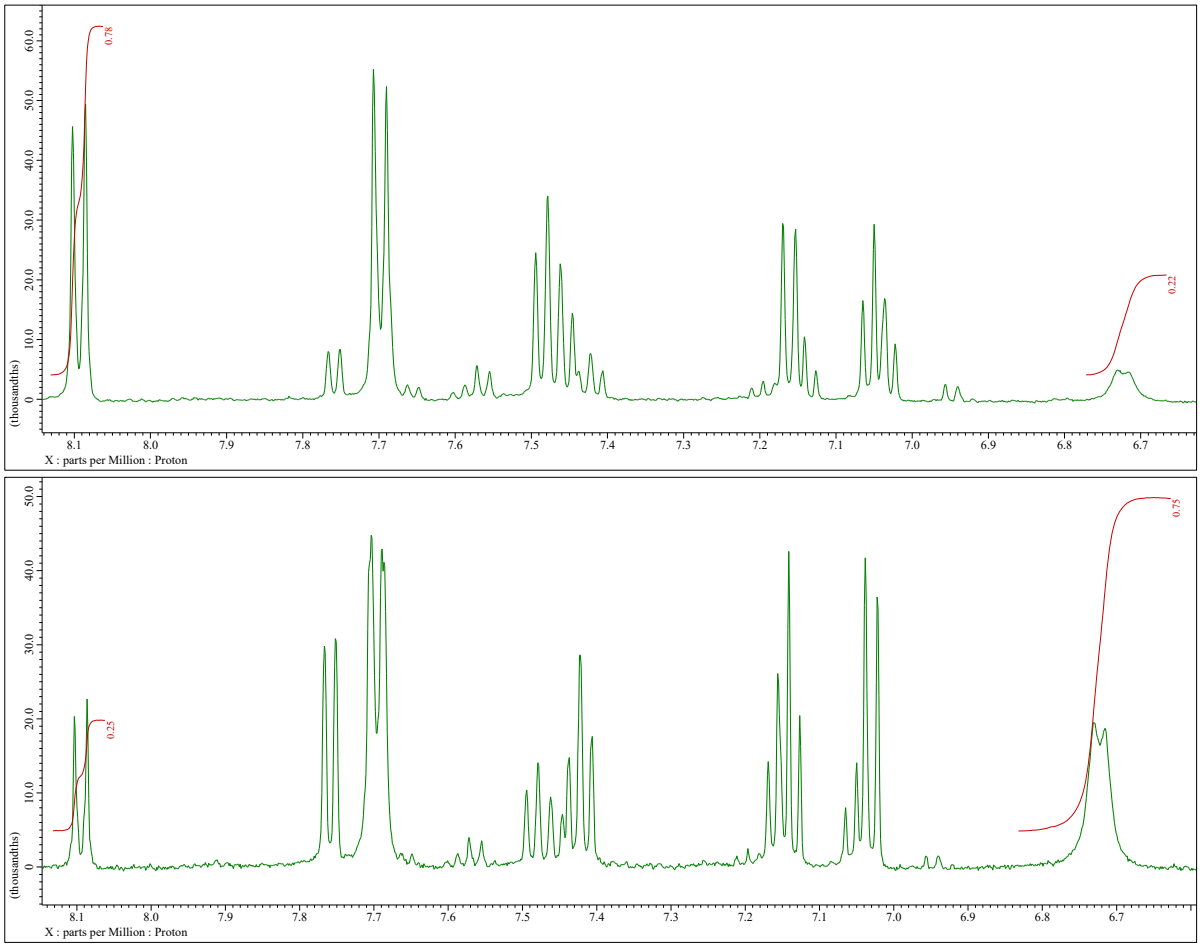

Figure S10. *^{1}H NMR spectra of the aromatic region of **Ar-Me** in dark (top) and under irradiation with 660 nm red light (bottom), showing a change from a dark equilibrium of 78:22 E:Z to a PSS of 25:75 E:Z.*

Absorption spectra and PSS

The absorption spectra of the studied indigo derivatives in dilute acetonitrile solutions are presented in **Fig. 1** in the manuscript and **Fig. S4**. The absorption spectra recorded in each polymeric environment are shown below. PSS distributions were calculated from the spectra as described above.

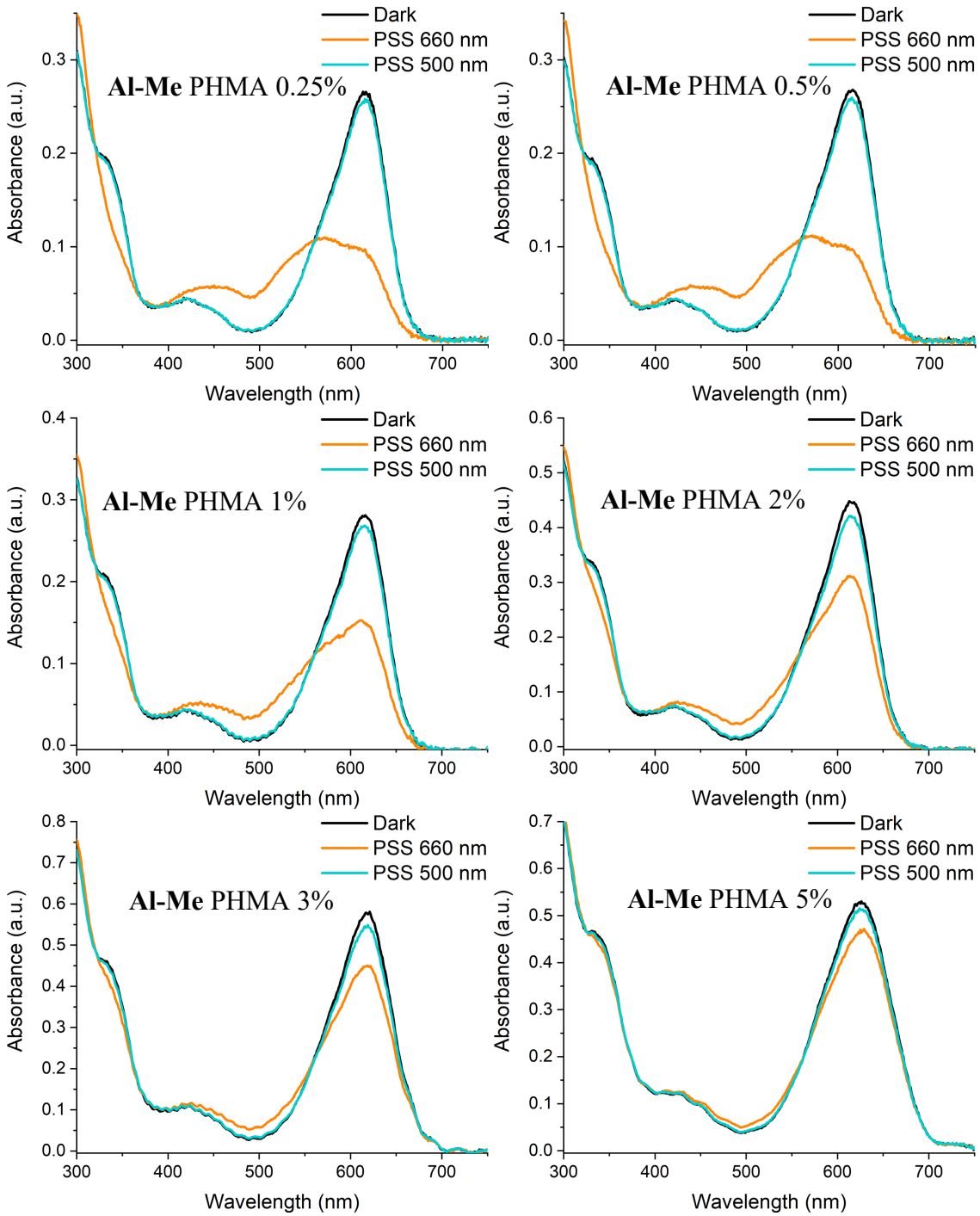

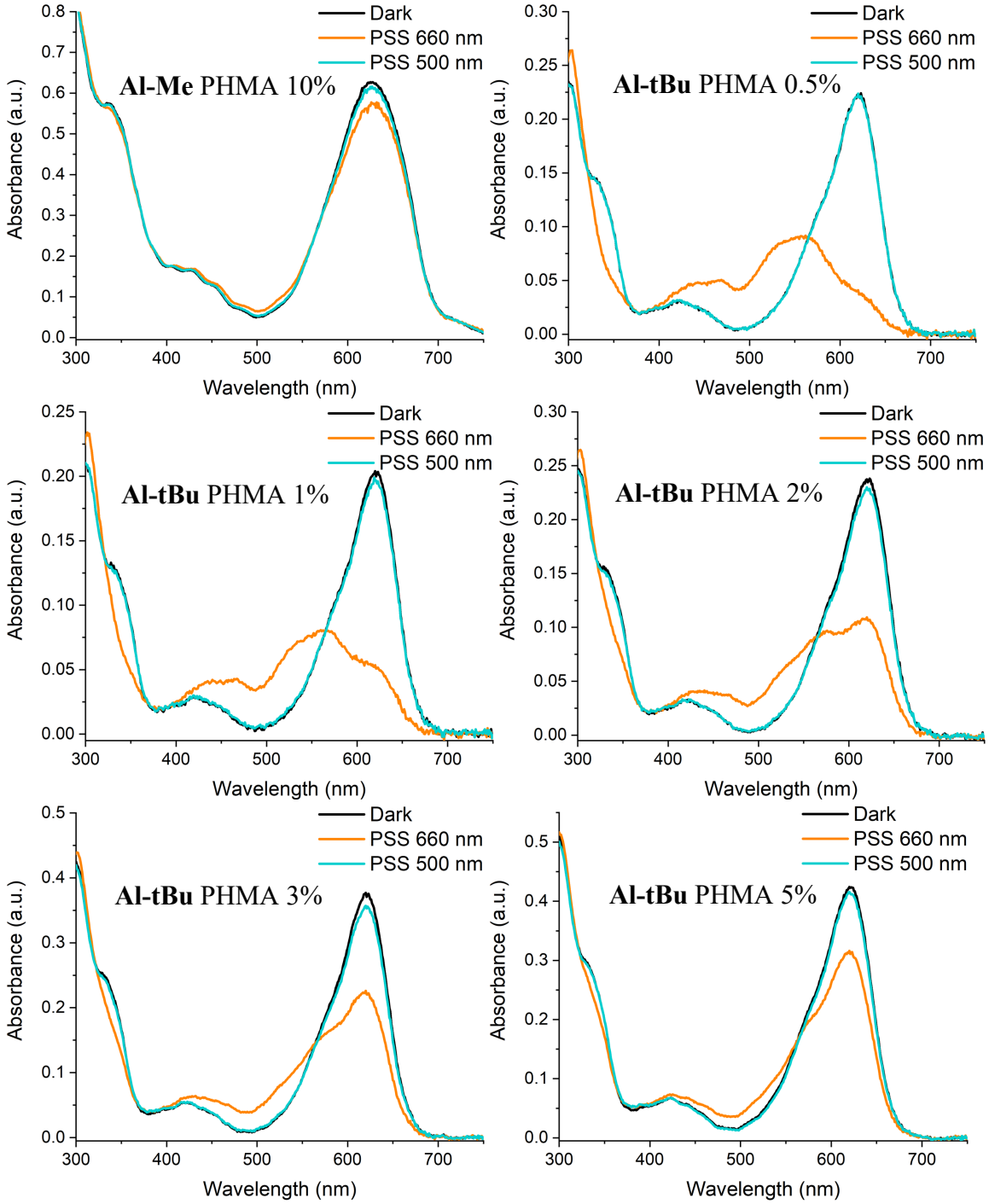
Dark
PSS 660 nm
PSS 500 nm
Al-Me PHMA 10%
Al-tBu PHMA 0.5%
Al-tBu PHMA 1%
Al-tBu PHMA 2%
Al-tBu PHMA 3%
Al-tBu PHMA 5%
Absorbance (a.u.)
Wavelength (nm)

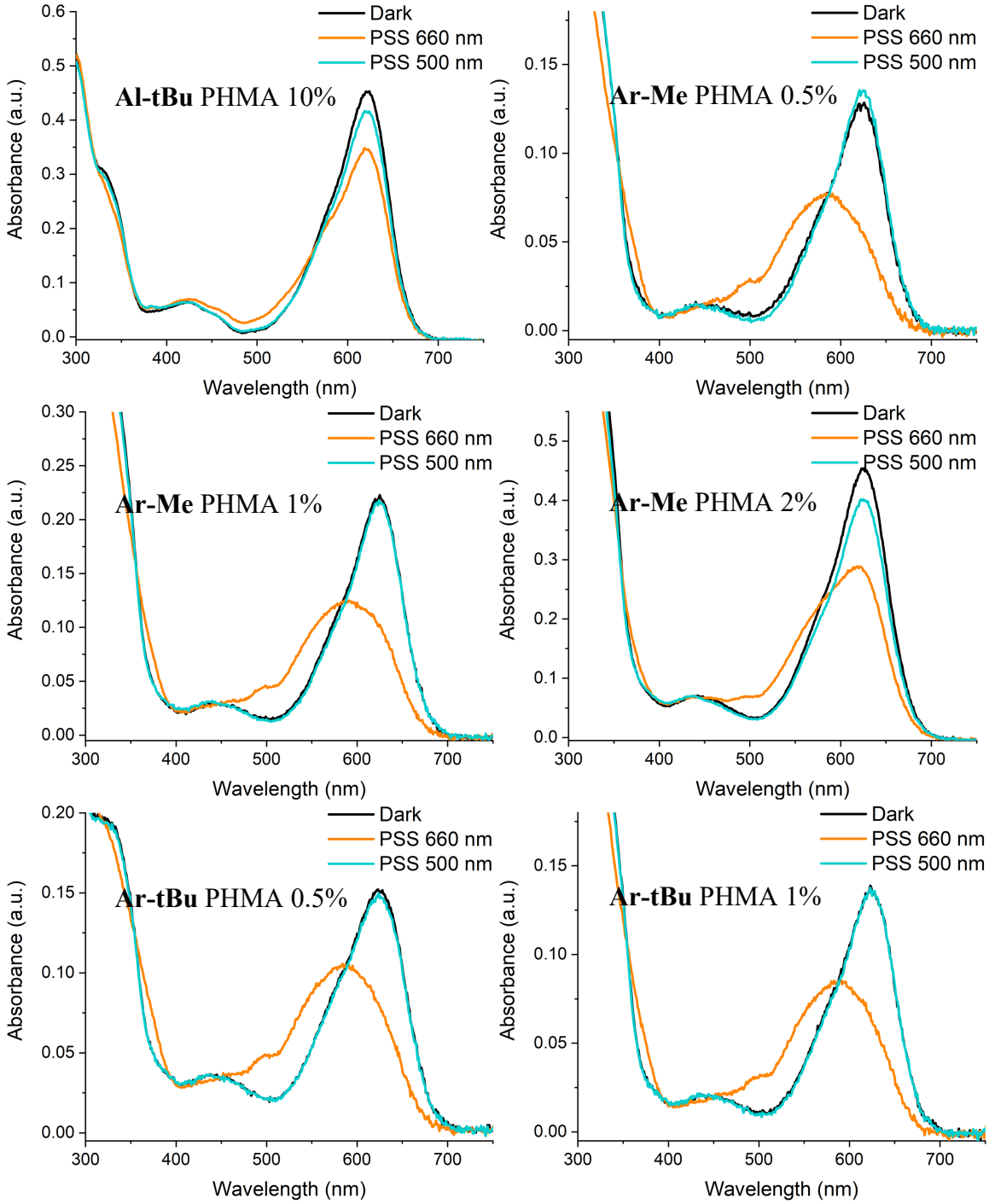
Dark
PSS 660 nm
PSS 500 nm
Al-tBu PHMA 10%
Ar-Me PHMA 0.5%
Ar-Me PHMA 1%
Ar-Me PHMA 2%
Ar-tBu PHMA 0.5%
Ar-tBu PHMA 1%
Absorbance (a.u.)
Wavelength (nm)

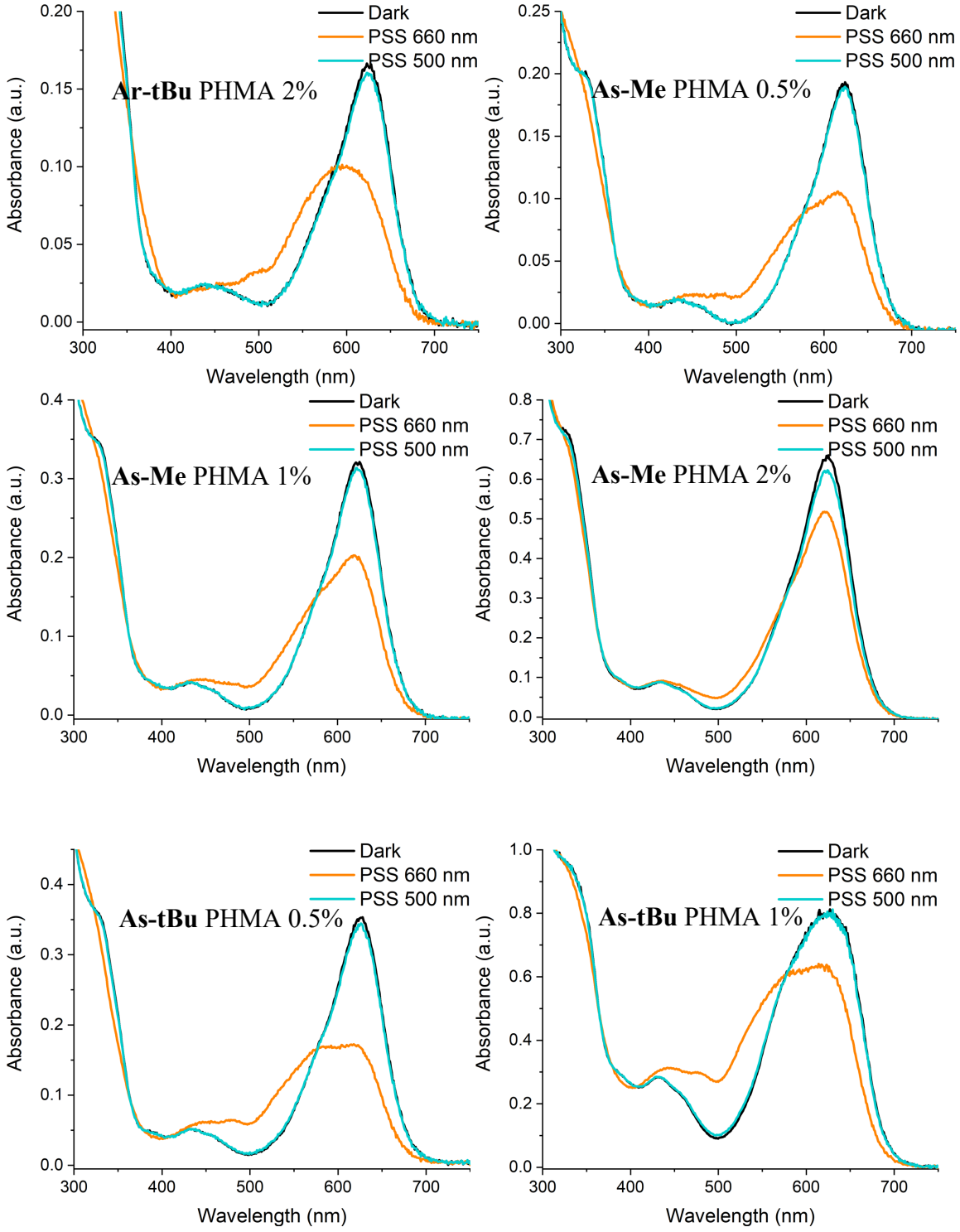
Ar-tBu PHMA 2%
As-Me PHMA 0.5%
As-Me PHMA 1%
As-Me PHMA 2%
As-tBu PHMA 0.5%
As-tBu PHMA 1%
Dark
PSS 660 nm
PSS 500 nm
Absorbance (a.u.)
Wavelength (nm)

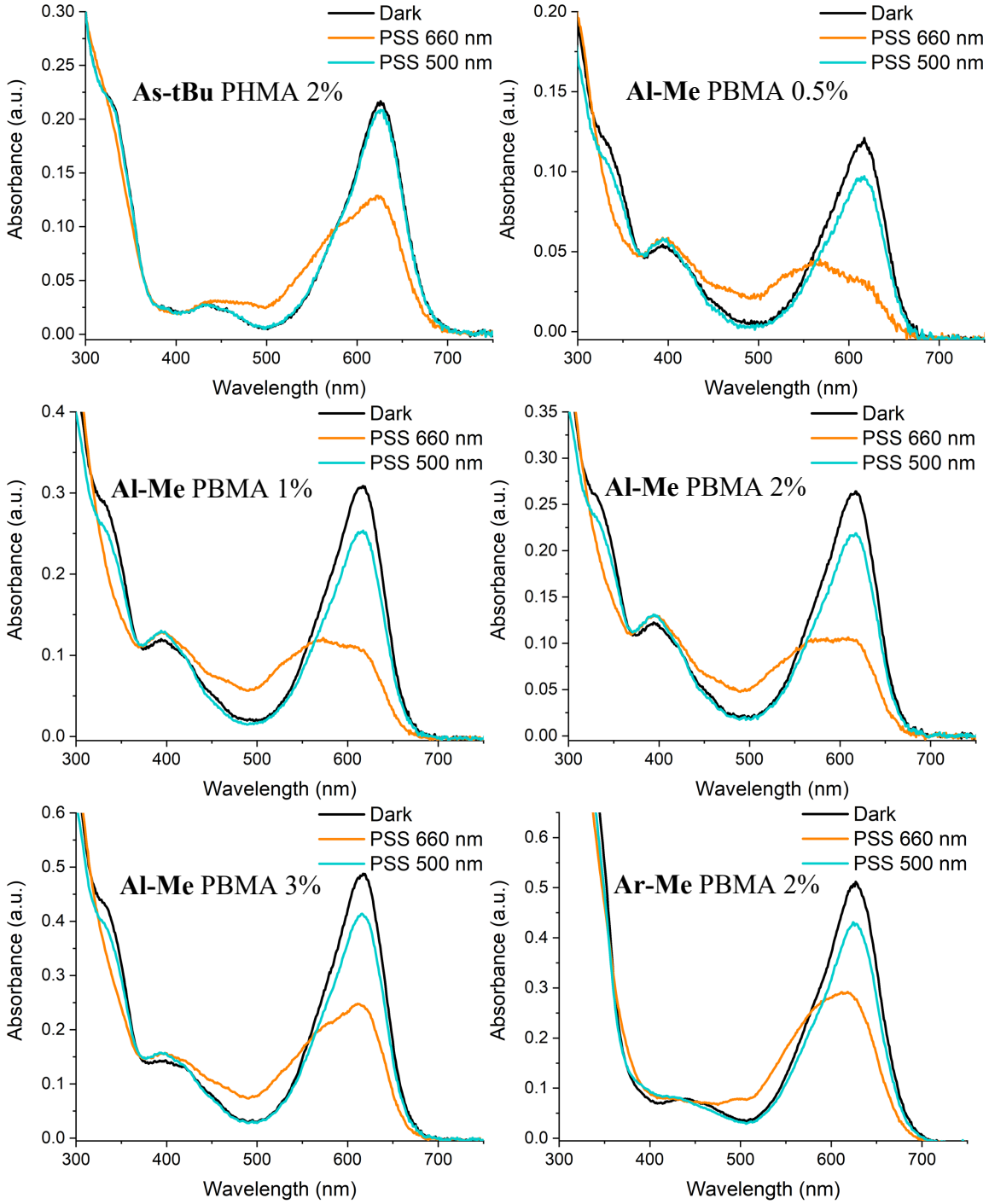
Dark
PSS 660 nm
PSS 500 nm
As-tBu PHMA 2%
Al-Me PBMA 0.5%
Al-Me PBMA 1%
Al-Me PBMA 2%
Al-Me PBMA 3%
Ar-Me PBMA 2%
Absorbance (a.u.)
Wavelength (nm)

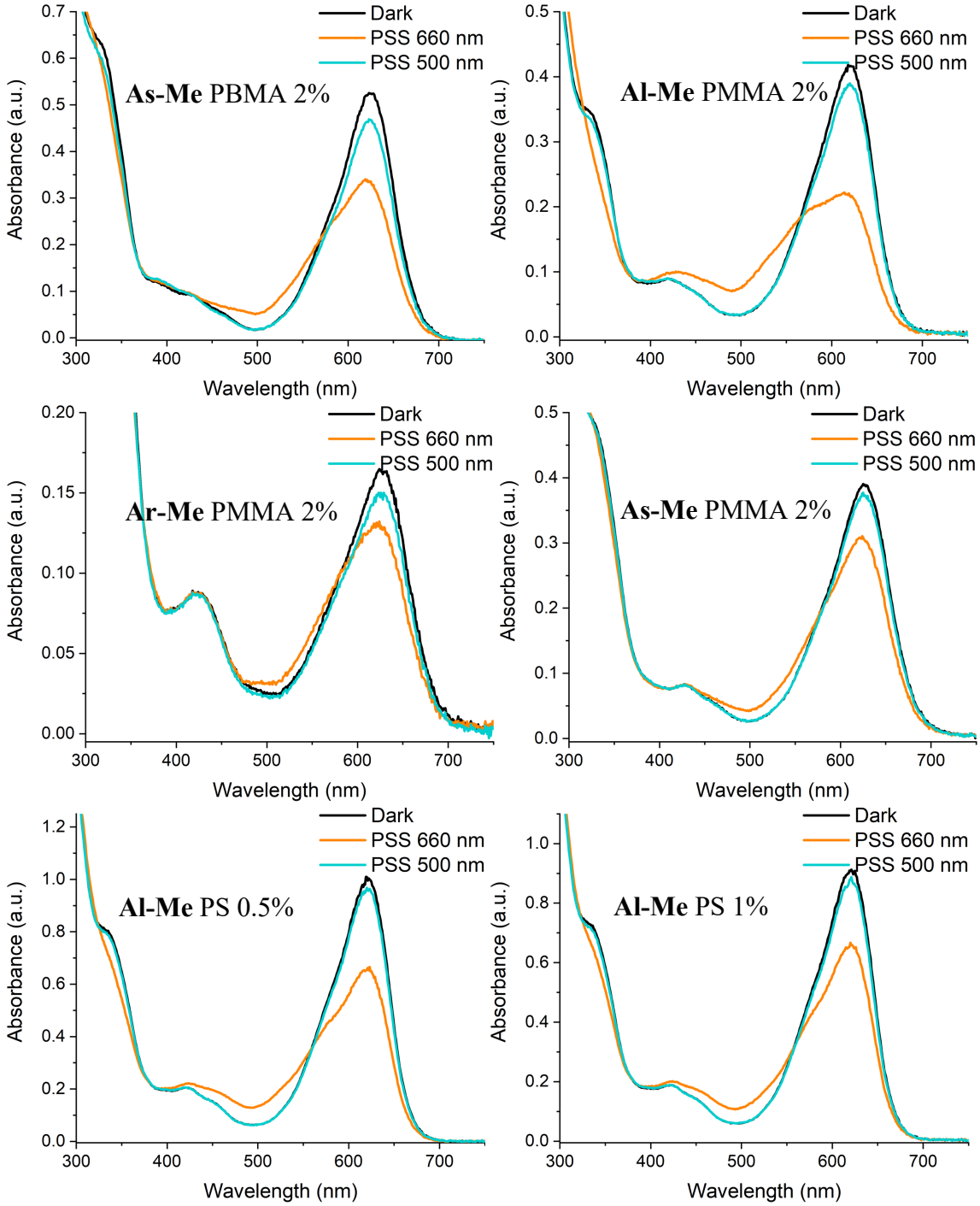
Dark
PSS 660 nm
PSS 500 nm
As-Me PBMA 2%
Al-Me PMMA 2%
Ar-Me PMMA 2%
As-Me PMMA 2%
Al-Me PS 0.5%
Al-Me PS 1%
Absorbance (a.u.)
Wavelength (nm)

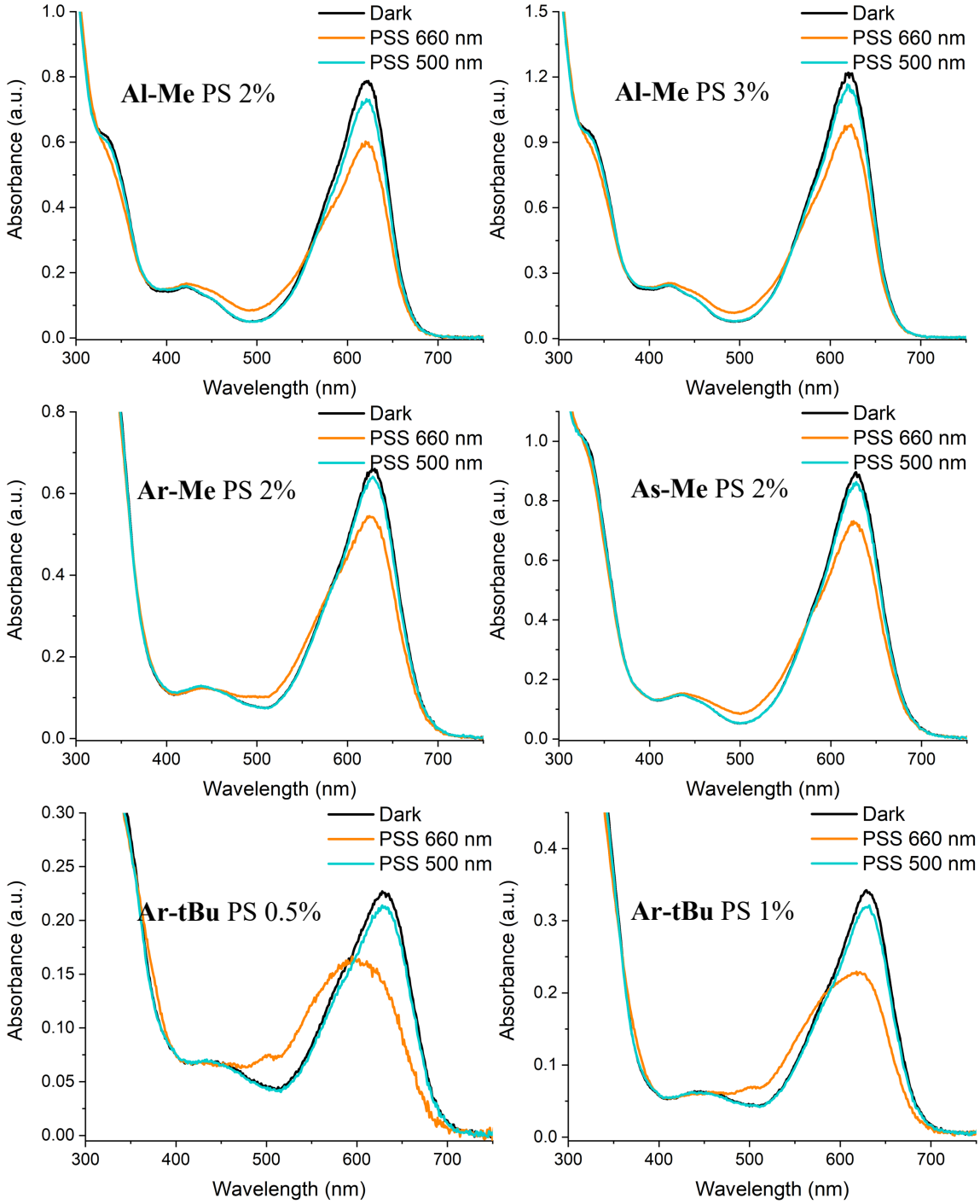
Dark
PSS 660 nm
PSS 500 nm
Al-Me PS 2%
Al-Me PS 3%
Ar-Me PS 2%
As-Me PS 2%
Ar-tBu PS 0.5%
Ar-tBu PS 1%
Absorbance (a.u.)
Wavelength (nm)

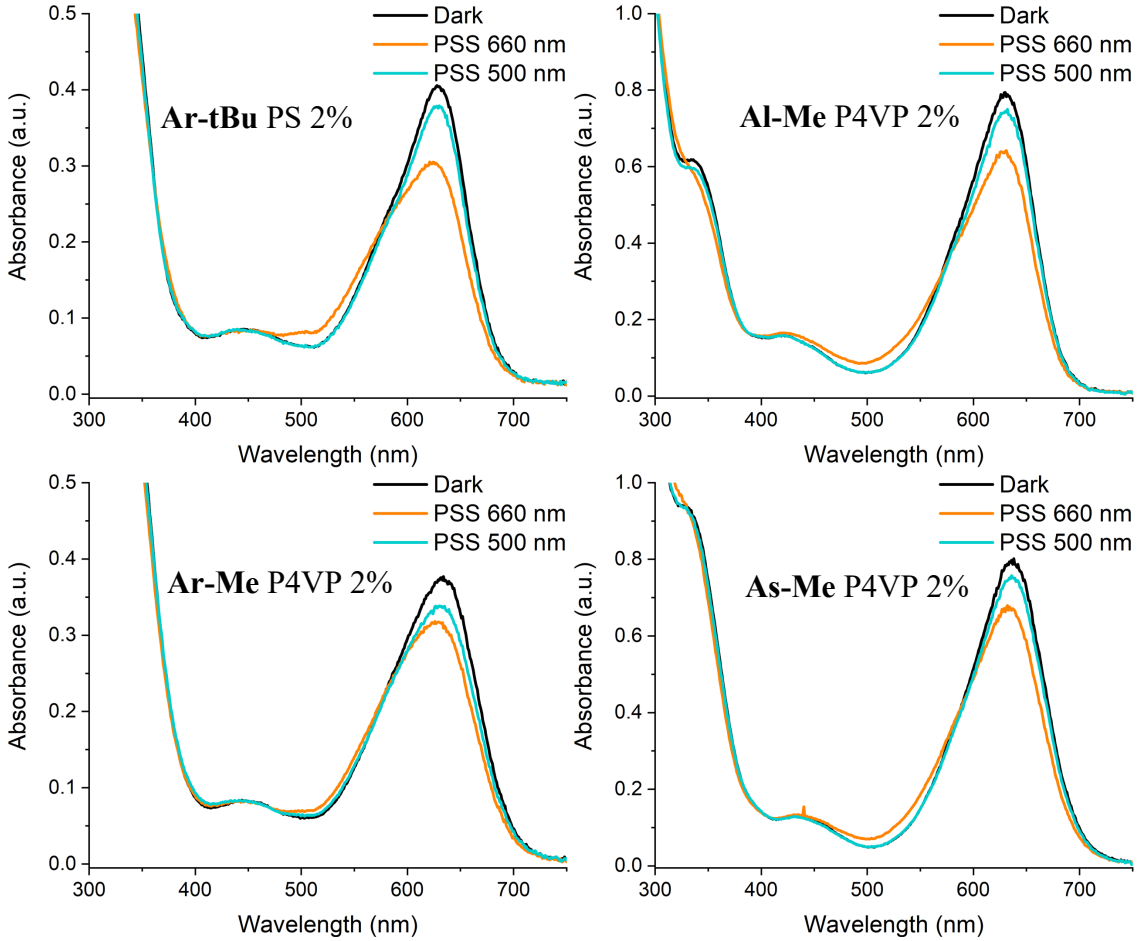
Dark
PSS 660 nm
PSS 500 nm
Ar-tBu PS 2%
Al-Me P4VP 2%
Ar-Me P4VP 2%
As-Me P4VP 2%
Absorbance (a.u.)
Wavelength (nm)

Thermal isomerisation

In solution, the thermal isomerisation of an indigo derivative from the metastable *Z* isomer to the stable *E* isomer (or to an equilibrium consisting of a mixture of both isomers) follows simple first order reaction kinetics. Thus, a monoexponential decay function can be used to describe the change in the concentration of either isomer over time. The concentration change can most easily be monitored by recording UV-vis spectra over time, since the two isomers have different absorption spectra and absorbance correlates with concentration as per the Beer-Lambert law. In the case of indigos, the spectral changes are largest near the peak of the major absorption band of the *E* isomer located in the red end of the spectrum. Hence, to study the isomerisation kinetics, we monitored the absorbance at 620–635 nm (depending on the indigo derivative) over time and fitted the data with the equation

$$A(t) = A_\infty - (A_\infty - A_0)e^{\frac{t-t_0}{\tau}}, \qquad \text{(Eq. 1)}$$

in which $A(t)$ is the absorbance at time t, A_∞ is the absorbance when the thermal isomerisation is complete, A_0 is the absorbance in the beginning of the measurement (t_0), and τ is the thermal lifetime of the *Z* isomer. It should be noted that this is not equal to the half-life of the isomer, although the latter can easily be calculated from τ (see below). Eq. 1 was used to fit the thermal isomerisation of the indigos in solution.

In a polymeric environment the individual indigo molecules do not share a homogenous environment. Instead, the microenvironment can differ greatly between two molecules, which affects their isomerisation. To account for this, we used a so-called stretched exponential function to fit the isomerisation data in polymers. The equation is otherwise similar to the monoexponential equation but contains a factor b:

$$A(t) = A_\infty - (A_\infty - A_0)e^{\left(\left(\frac{t-t_0}{\tau}\right)^b\right)} \qquad \text{(Eq. 2)}$$

The fitting parameters of all thermal isomerisation measurements are presented in **Table S4**. The half-life was calculated from Eq. 1 or 2. For solution studies, Eq. 1 can be used and the half-life is

$$t_{1/2} = \tau \ln(2), \qquad \text{(Eq. 3)}$$

whereas for the polymer studies, the stretch factor must be accounted for and from Eq. 2:

$$t_{1/2} = \tau\,(\ln(2))^{1/b}. \qquad \text{(Eq. 4)}$$

Note that in the fitting graphs, the fitting function is of the form

$$y = y_0 + A\,e^{\left(\frac{x-x_0}{\tau}\right)^b}, \qquad \text{(Eq. 5)}$$

so compared to Eq. 2, y_0 is equal to A_∞, A is equal to $-(A_\infty - A_0)$, and $x - x_0$ is equal to $t - t_0$.

The utility of a stretched exponential fit (as compared to a non-stretched monoexponential fit) is demonstrated by **Figure S11**.

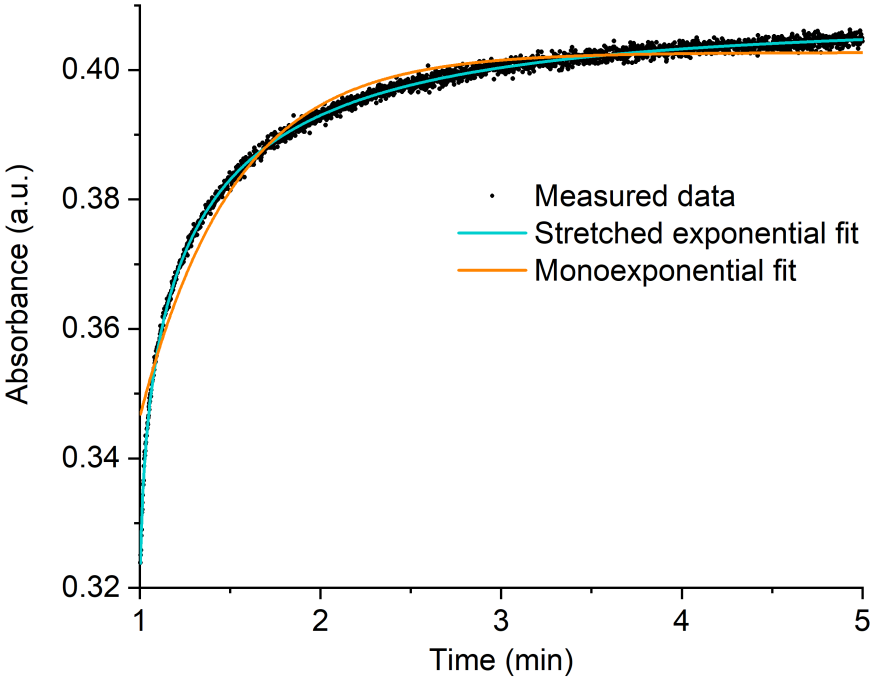

***Figure S11**. A comparison of a stretched exponential fit and a monoexponential fit (**Al-tBu** in PHMA, 10%). Here, the stretch factor b is 0.47. The stretched function performs better especially in the beginning of the isomerisation.*

In one case (**Ar-Me** in P4VP, 2%) we were not able to get a satisfactory fit with the stretched exponential function. In this case, we used a biexponential fit to be able to present a reasonable half-life:

$$A(t) = A_\infty + A_1 e^{\frac{t-t_0}{\tau_1}} + A_2 e^{\frac{t-t_0}{\tau_2}} \qquad \text{(Eq. 6)}$$

For discussion purposes, the energy differences between thermal isomerisation barriers ($\Delta\Delta G^\ddagger$) were approximated using the Eyring equation, with the approximation of $\kappa = 1$:

$$\Delta G^\ddagger = RT \ln\left(\frac{kh}{k_B T \kappa}\right) \qquad \text{(Eq. 7)}$$

Here, k is the fitted rate constant, h is the Planck constant, k_B is the Boltzmann constant, and T is temperature.

***Table S3**. Fitting parameters of thermal isomerisation for each polymer–indigo combination: the constant A_∞ (y_0 in the fits), preexponential factor **A**, the lifetime τ, goodness of fit value R^2, stretch factor **b**, and thermal half-life $t_{1/2}$. See the text above for the explanations of each parameter.*

		c_{indigo}	A_∞	A	τ (min)	R^2	*b*	$t_{1/2}$ (min)
Al-Me	MeCN	50 µM	0.71072	-1.52166	2.08±0.001	0.99997	1	1.441
Ar-Me	MeCN	50 µM	0.42871	-0.17257	58.87±2.644	0.99889	1	40.806
As-Me	MeCN	50 µM	0.63301	-0.35473	5.49±0.049	0.99934	1	3.807
Al-tBu	MeCN	50 µM	0.7004	-0.9998	3.55±0.001	0.99998	1	2.459
Ar-tBu	MeCN	50 µM	0.68958	-0.34618	37.5±0.317	0.99891	1	25.99
As-tBu	MeCN	50 µM	0.58559	-0.35762	5.56±0.043	0.99949	1	3.857
Al-Me	P4VP	2 %	0.24716	-0.02598	2.71±0.964	0.97444	0.48368	1.27
Ar-Me	P4VP	2 %	*0.34024*	*-0.02537*	*615±2040*	*0.98569*	*0.26895*	10.9[a]
As-Me	P4VP	2 %	0.73168	-0.06764	25.59±18.50	0.99244	0.3467	8.89
Al-Me	PS	2 %	0.82319	-0.20667	2.24±0.351	0.99535	0.27593	0.593
Ar-Me	PS	2 %	0.6068	-0.06965	70.85±74.464	0.97484	0.41615	29.365
As-Me	PS	2 %	0.87818	-0.13929	31.78±0.101	0.99798	0.40033	12.723
Ar-tBu	PS	0.5 %	0.14224	-0.06028	894±146	0.99394	0.86159	584.227
Al-Me	PMMA	2 %	0.34921	-0.11194	1.23±0.006	0.99983	0.59877	0.667
Ar-Me	PMMA	2 %	0.14217	-0.01202	34.84±10.311	0.98321	0.79508	21.971
As-Me	PMMA	2 %	0.24709	-0.04192	7.6±0.088	0.98389	0.65178	4.33
Al-Me	PBMA	2 %	0.25544	-0.14154	1.28±0.001	0.99988	0.89488	0.847
Ar-Me	PBMA	2 %	0.39023	-0.12838	153.9±23.3	0.99799	0.88744	101.822
As-Me	PBMA	2 %	0.50557	-0.13231	12.95±4.186	0.99626	0.84497	8.392
Al-Me	PHMA	0.25 %	0.24794	-0.15709	0.94±0.001	0.99978	0.80766	0.599
Al-Me	PHMA	0.5 %	0.25198	-0.16489	1.01±0.001	0.99981	0.83116	0.647
Al-Me	PHMA	1 %	0.28638	-0.13472	0.6±0.001	0.99943	0.68677	0.351
Al-Me	PHMA	2 %	0.40887	-0.13934	0.41±0.002	0.99921	0.57863	0.215
Al-Me	PHMA	3 %	0.5455	-0.16865	0.08±0.006	0.99738	0.4225	0.036
Al-Me	PHMA	5 %	0.52333	-0.0953	0.05±0.007	0.97926	0.31335	0.016
Al-Me	PHMA	10 %	0.60306	-0.05393	0.05±0.017	0.98669	0.12141	0.002
Al-tBu	PHMA	0.5 %	0.24129	-0.19609	6.9±0.017	0.9999	0.88234	4.553
Al-tBu	PHMA	1 %	0.20389	-0.15624	5.49±0.006	0.99985	0.72658	3.318
Al-tBu	PHMA	2 %	0.22873	-0.12711	3.07±0.005	0.99957	0.60718	1.679
Al-tBu	PHMA	3 %	0.35904	-0.15005	1.17±0.003	0.99942	0.55716	0.608
Al-tBu	PHMA	5 %	0.44723	-0.13838	0.69±0.003	0.99894	0.47069	0.318
Al-tBu	PHMA	10 %	0.40716	-0.09667	0.25±0.003	0.99749	0.46733	0.113
Ar-Me	PHMA	2 %	0.38218	-0.12528	69.65±4.695	0.99868	0.86715	45.643
As-Me	PHMA	2 %	1.00463	-0.11551	2.28±0.02	0.9973	0.43749	0.986

[a] Half-life calculated from a biexponential fit $A(t) = 0.32953 - 0.0064e^{\frac{t-0.5\,\text{min}}{1.37502\,\text{min}}} - 0.00789e^{\frac{t-0.5\,\text{min}}{109.587\,\text{min}}}$

The thermal isomerisation graphs are shown below.

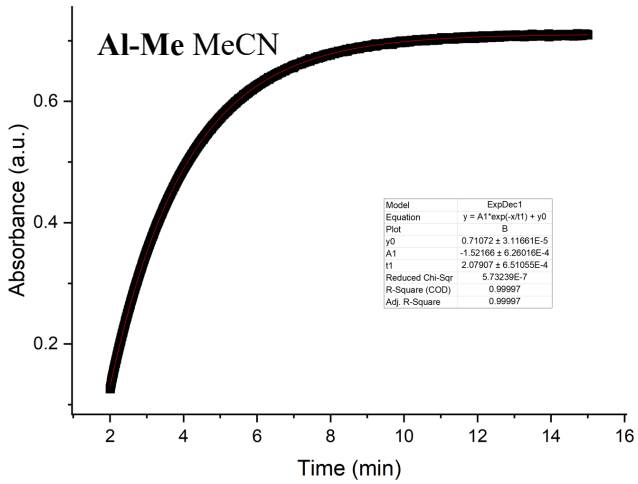
Al-Me MeCN
Absorbance (a.u.)
Time (min)
Model ExpDec1
Equation y = A1*exp(-x/t1) + y0
Plot B
y0 0.71072 ± 3.11661E-5
A1 -1.52166 ± 6.26016E-4
t1 2.07907 ± 6.51055E-4
Reduced Chi-Sqr 5.73239E-7
R-Square (COD) 0.99997
Adj. R-Square 0.99997

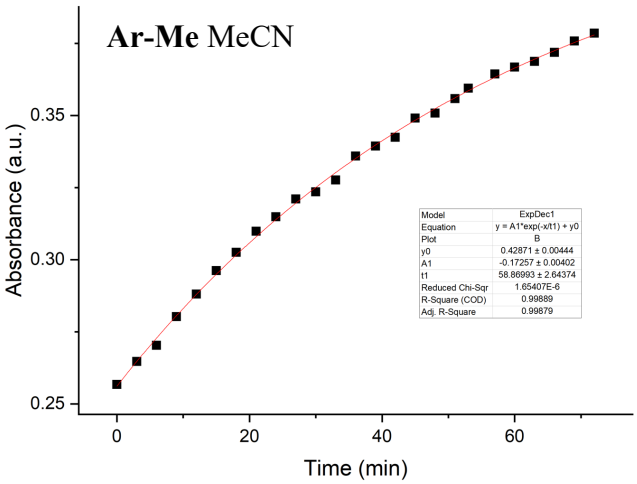
Ar-Me MeCN
Absorbance (a.u.)
Time (min)
Model ExpDec1
Equation y = A1*exp(-x/t1) + y0
Plot B
y0 0.42871 ± 0.00444
A1 -0.17257 ± 0.00402
t1 58.86993 ± 2.64374
Reduced Chi-Sqr 1.65407E-6
R-Square (COD) 0.99889
Adj. R-Square 0.99879

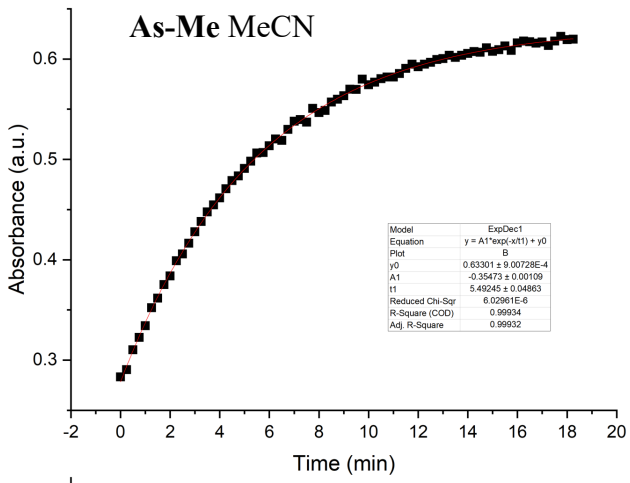
As-Me MeCN
Absorbance (a.u.)
Time (min)
Model ExpDec1
Equation y = A1*exp(-x/t1) + y0
Plot B
y0 0.63301 ± 9.00728E-4
A1 -0.35473 ± 0.00109
t1 5.49245 ± 0.04863
Reduced Chi-Sqr 6.02961E-6
R-Square (COD) 0.99934
Adj. R-Square 0.99932

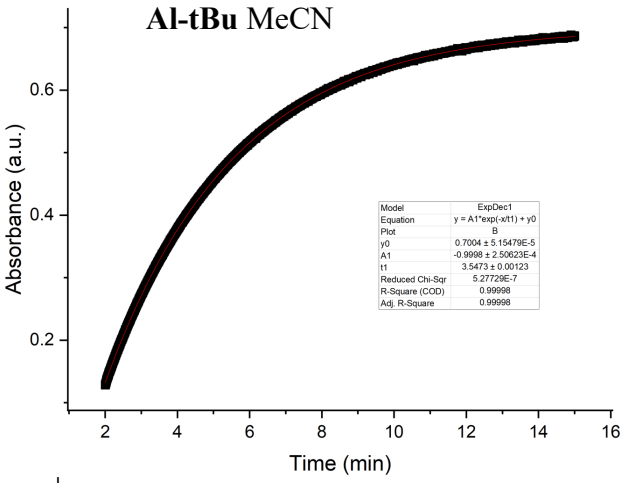
Al-tBu MeCN
Absorbance (a.u.)
Time (min)
Model ExpDec1
Equation y = A1*exp(-x/t1) + y0
Plot B
y0 0.7004 ± 5.15479E-5
A1 -0.9998 ± 2.50623E-4
t1 3.5473 ± 0.00123
Reduced Chi-Sqr 5.27729E-7
R-Square (COD) 0.99998
Adj. R-Square 0.99998

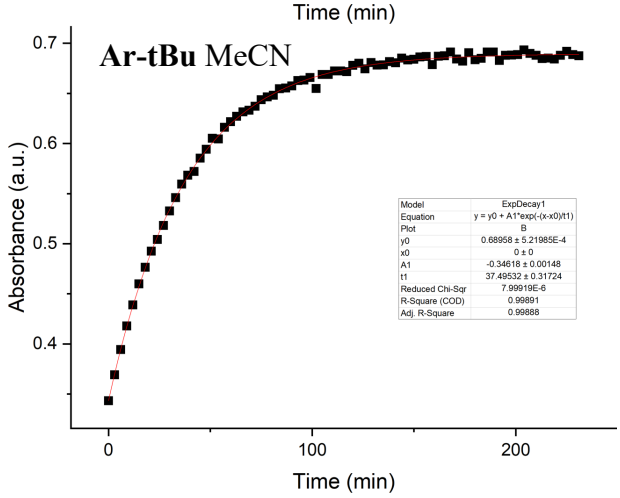
Ar-tBu MeCN
Absorbance (a.u.)
Time (min)
Model ExpDecay1
Equation y = y0 + A1*exp(-(x-x0)/t1)
Plot B
y0 0.68958 ± 5.21985E-4
x0 0 ± 0
A1 -0.34618 ± 0.00148
t1 37.49532 ± 0.31724
Reduced Chi-Sqr 7.99919E-6
R-Square (COD) 0.99891
Adj. R-Square 0.99888

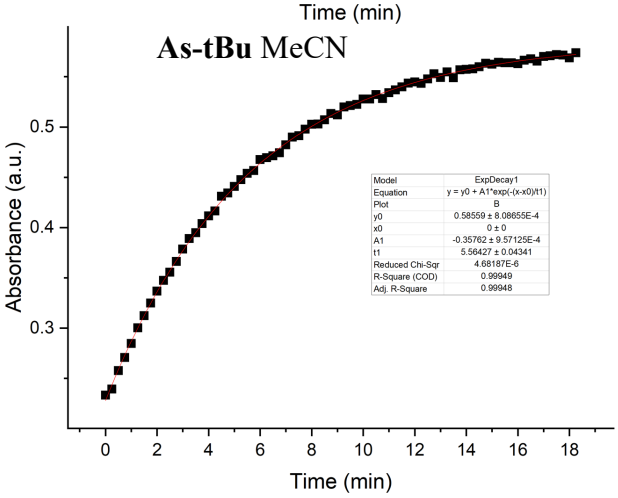
As-tBu MeCN
Absorbance (a.u.)
Time (min)
Model ExpDecay1
Equation y = y0 + A1*exp(-(x-x0)/t1)
Plot B
y0 0.58559 ± 8.08655E-4
x0 0 ± 0
A1 -0.35762 ± 9.57125E-4
t1 5.56427 ± 0.04341
Reduced Chi-Sqr 4.68187E-6
R-Square (COD) 0.99949
Adj. R-Square 0.99948

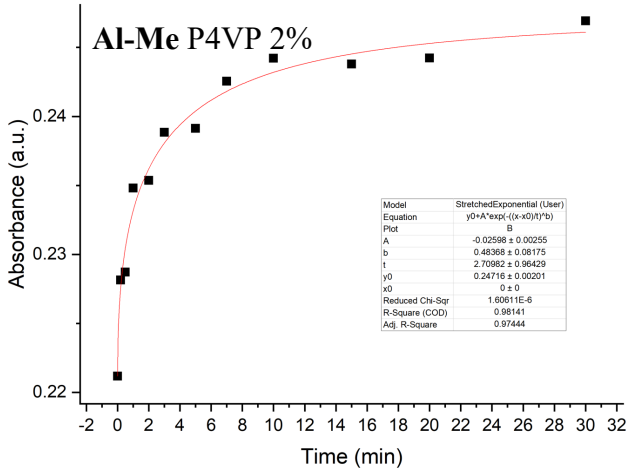
Al-Me P4VP 2%
Absorbance (a.u.)
Time (min)
Model StretchedExponential (User)
Equation y0+A*exp(-((x-x0)/t)^b)
Plot B
A -0.02598 ± 0.00255
b 0.48368 ± 0.08175
t 2.70982 ± 0.96429
y0 0.24716 ± 0.00201
x0 0 ± 0
Reduced Chi-Sqr 1.60611E-6
R-Square (COD) 0.98141
Adj. R-Square 0.97444

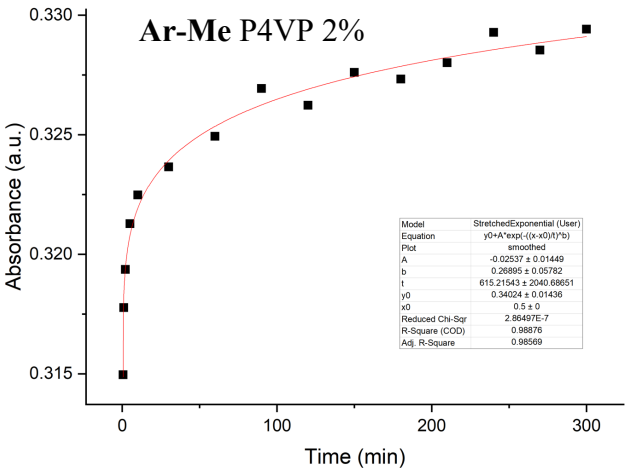
Ar-Me P4VP 2%
Absorbance (a.u.)
Time (min)
Model StretchedExponential (User)
Equation y0+A*exp(-((x-x0)/t)^b)
Plot smoothed
A -0.02537 ± 0.01449
b 0.26895 ± 0.05782
t 615.21543 ± 2040.68651
y0 0.34024 ± 0.01436
x0 0.5 ± 0
Reduced Chi-Sqr 2.86497E-7
R-Square (COD) 0.98876
Adj. R-Square 0.98569

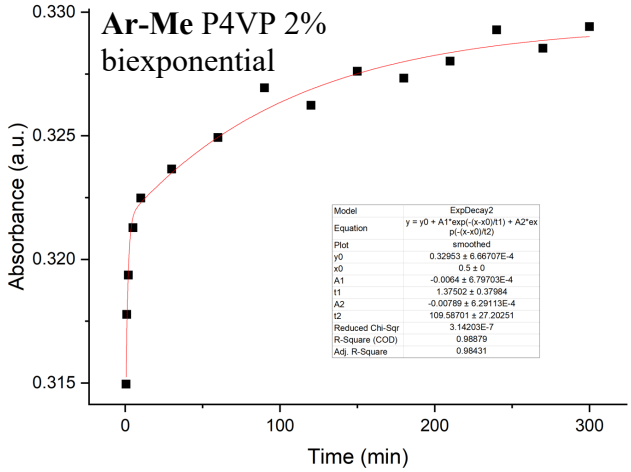
Ar-Me P4VP 2%
biexponential
Absorbance (a.u.)
Time (min)
Model ExpDecay2
Equation y = y0 + A1*exp(-(x-x0)/t1) + A2*exp(-(x-x0)/t2)
Plot smoothed
y0 0.32953 ± 6.66707E-4
x0 0.5 ± 0
A1 -0.0064 ± 6.79703E-4
t1 1.37502 ± 0.37984
A2 -0.00789 ± 6.29113E-4
t2 109.58701 ± 27.20251
Reduced Chi-Sqr 3.14203E-7
R-Square (COD) 0.98879
Adj. R-Square 0.98431

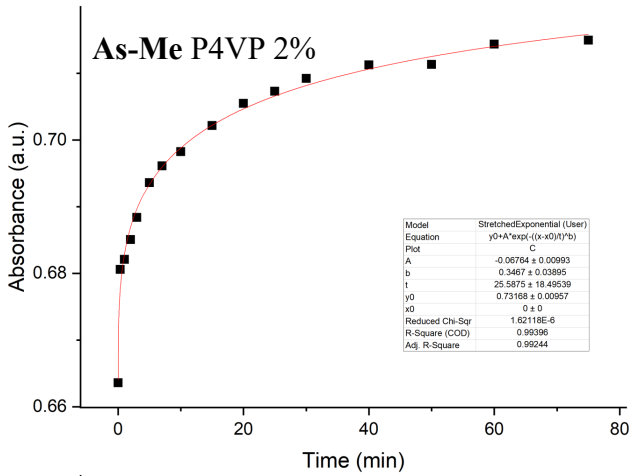
As-Me P4VP 2%
Absorbance (a.u.)
Time (min)
Model StretchedExponential (User)
Equation y0+A*exp(-((x-x0)/t)^b)
Plot C
A -0.06764 ± 0.00993
b 0.3467 ± 0.03895
t 25.5875 ± 18.49539
y0 0.73168 ± 0.00957
x0 0 ± 0
Reduced Chi-Sqr 1.62118E-6
R-Square (COD) 0.99396
Adj. R-Square 0.99244

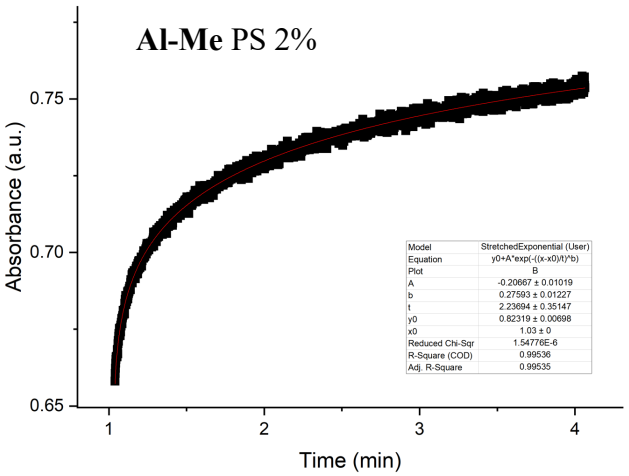
Al-Me PS 2%
Absorbance (a.u.)
Time (min)
Model StretchedExponential (User)
Equation y0+A*exp(-((x-x0)/t)^b)
Plot B
A -0.20667 ± 0.01019
b 0.27593 ± 0.01227
t 2.23694 ± 0.35147
y0 0.82319 ± 0.00698
x0 1.03 ± 0
Reduced Chi-Sqr 1.54776E-6
R-Square (COD) 0.99536
Adj. R-Square 0.99535

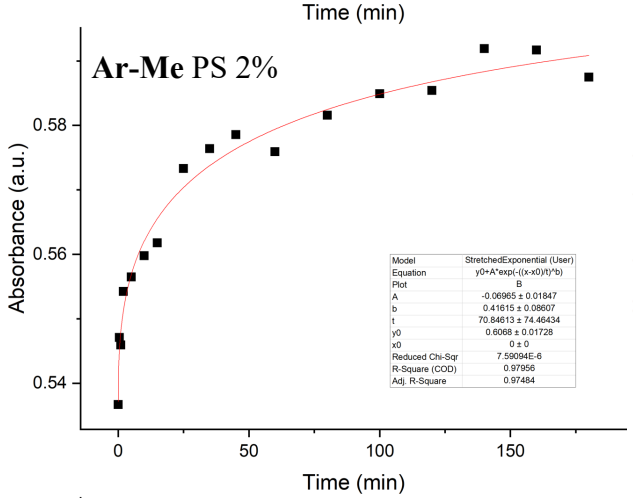
Ar-Me PS 2%
Absorbance (a.u.)
Time (min)
Model StretchedExponential (User)
Equation y0+A*exp(-((x-x0)/t)^b)
Plot B
A -0.06965 ± 0.01847
b 0.41615 ± 0.08607
t 70.84613 ± 74.46434
y0 0.6068 ± 0.01728
x0 0 ± 0
Reduced Chi-Sqr 7.59094E-6
R-Square (COD) 0.97956
Adj. R-Square 0.97484

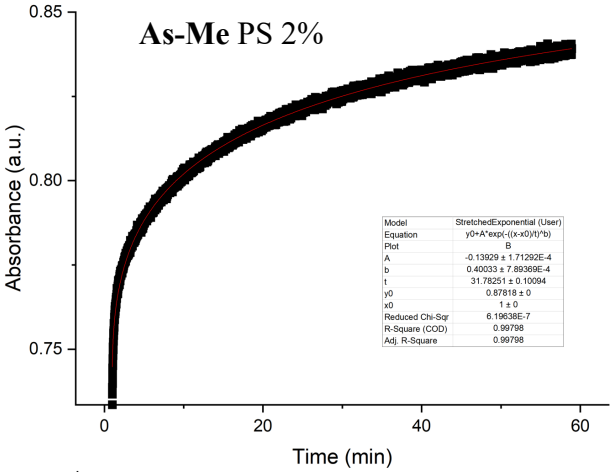
As-Me PS 2%
Absorbance (a.u.)
Time (min)
Model StretchedExponential (User)
Equation y0+A*exp(-((x-x0)/t)^b)
Plot B
A -0.13929 ± 1.71292E-4
b 0.40033 ± 7.89369E-4
t 31.78251 ± 0.10094
y0 0.87818 ± 0
x0 1 ± 0
Reduced Chi-Sqr 6.19638E-7
R-Square (COD) 0.99798
Adj. R-Square 0.99798

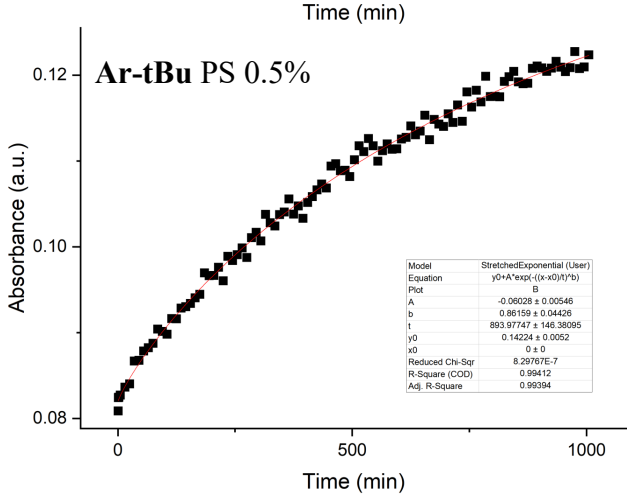
Ar-tBu PS 0.5%
Absorbance (a.u.)
Time (min)
Model StretchedExponential (User)
Equation y0+A*exp(-((x-x0)/t)^b)
Plot B
A -0.06028 ± 0.00546
b 0.86159 ± 0.04426
t 893.97747 ± 146.38095
y0 0.14224 ± 0.0052
x0 0 ± 0
Reduced Chi-Sqr 8.29767E-7
R-Square (COD) 0.99412
Adj. R-Square 0.99394

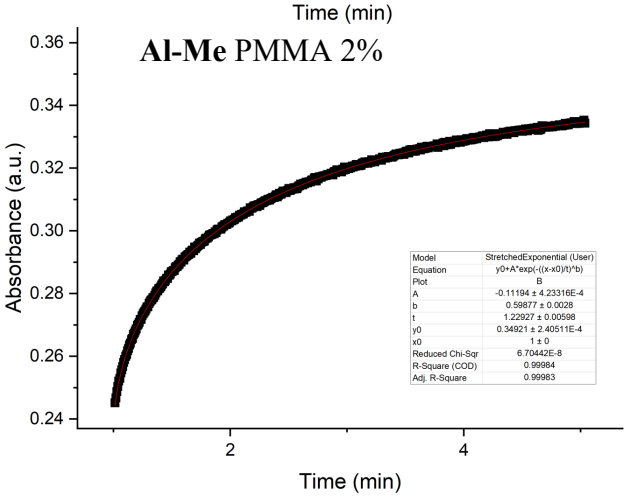
Al-Me PMMA 2%
Absorbance (a.u.)
Time (min)
Model StretchedExponential (User)
Equation y0+A*exp(-((x-x0)/t)^b)
Plot B
A -0.11194 ± 4.23316E-4
b 0.59877 ± 0.0028
t 1.22927 ± 0.00598
y0 0.34921 ± 2.40511E-4
x0 1 ± 0
Reduced Chi-Sqr 6.70442E-8
R-Square (COD) 0.99984
Adj. R-Square 0.99983

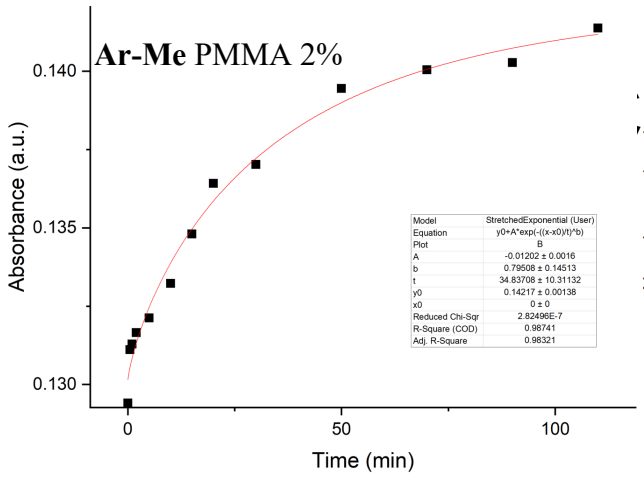
Ar-Me PMMA 2%
Absorbance (a.u.)
Time (min)
Model StretchedExponential (User)
Equation y0+A*exp(-((x-x0)/t)^b)
Plot B
A -0.01202 ± 0.0016
b 0.79508 ± 0.14513
t 34.83708 ± 10.31132
y0 0.14217 ± 0.00138
x0 0 ± 0
Reduced Chi-Sqr 2.82496E-7
R-Square (COD) 0.98741
Adj. R-Square 0.98321

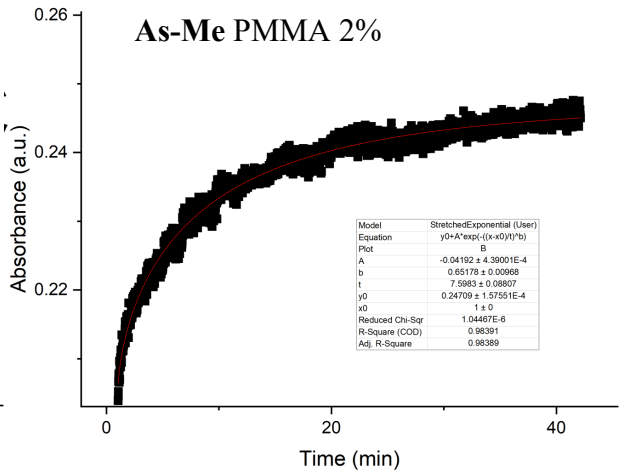
As-Me PMMA 2%
Absorbance (a.u.)
Time (min)
Model StretchedExponential (User)
Equation y0+A*exp(-((x-x0)/t)^b)
Plot B
A -0.04192 ± 4.39001E-4
b 0.65178 ± 0.00968
t 7.5983 ± 0.08807
y0 0.24709 ± 1.57551E-4
x0 1 ± 0
Reduced Chi-Sqr 1.04467E-6
R-Square (COD) 0.98391
Adj. R-Square 0.98389

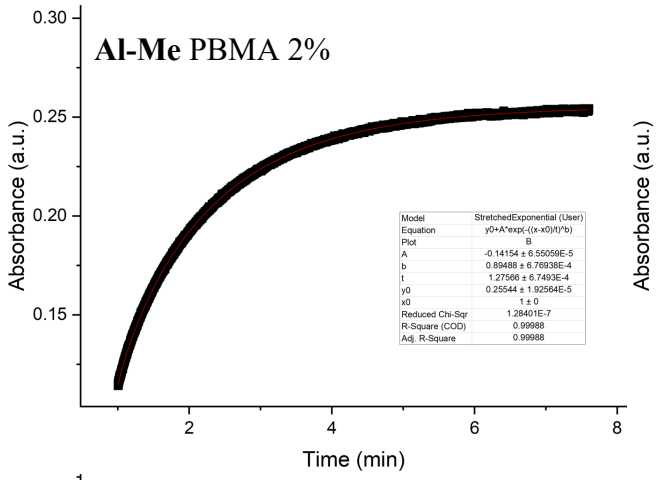
Al-Me PBMA 2%
Absorbance (a.u.)
Time (min)
Model StretchedExponential (User)
Equation y0+A*exp(-((x-x0)/t)^b)
Plot B
A -0.14154 ± 6.55059E-5
b 0.89488 ± 6.76938E-4
t 1.27566 ± 6.7493E-4
y0 0.25544 ± 1.92564E-5
x0 1 ± 0
Reduced Chi-Sqr 1.28401E-7
R-Square (COD) 0.99988
Adj. R-Square 0.99988

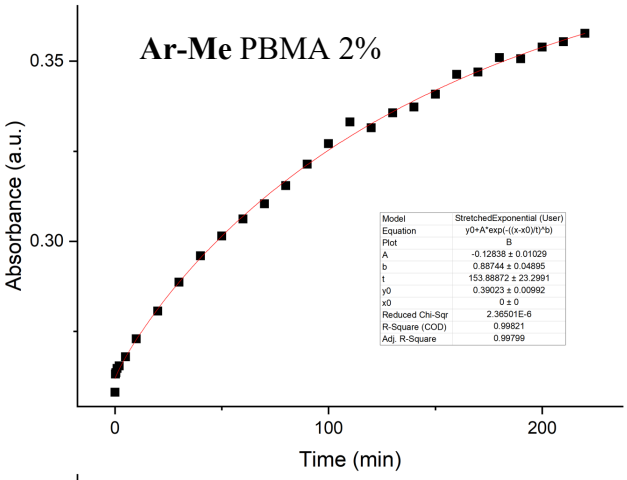
Ar-Me PBMA 2%
Absorbance (a.u.)
Time (min)
Model StretchedExponential (User)
Equation y0+A*exp(-((x-x0)/t)^b)
Plot B
A -0.12838 ± 0.01029
b 0.88744 ± 0.04895
t 153.88872 ± 23.2991
y0 0.39023 ± 0.00992
x0 0 ± 0
Reduced Chi-Sqr 2.36501E-6
R-Square (COD) 0.99821
Adj. R-Square 0.99799

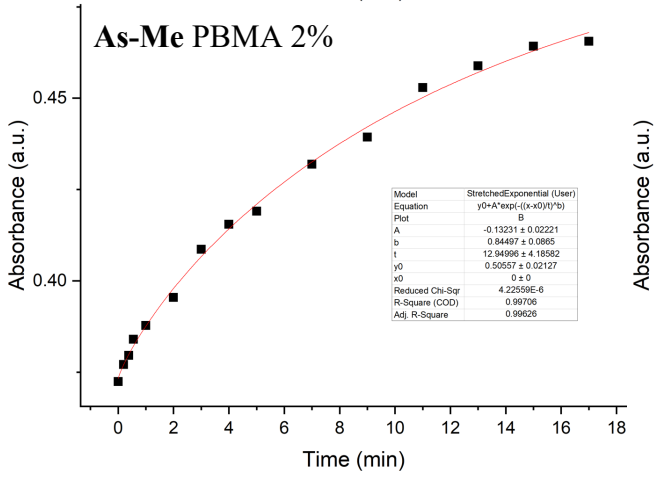
As-Me PBMA 2%
Absorbance (a.u.)
Time (min)
Model StretchedExponential (User)
Equation y0+A*exp(-((x-x0)/t)^b)
Plot B
A -0.13231 ± 0.02221
b 0.84497 ± 0.0865
t 12.94996 ± 4.18582
y0 0.50557 ± 0.02127
x0 0 ± 0
Reduced Chi-Sqr 4.22559E-6
R-Square (COD) 0.99706
Adj. R-Square 0.99626

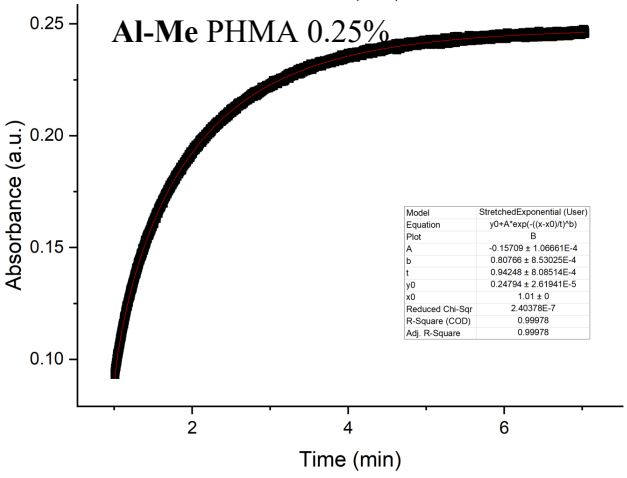
Al-Me PHMA 0.25%
Absorbance (a.u.)
Time (min)
Model StretchedExponential (User)
Equation y0+A*exp(-((x-x0)/t)^b)
Plot B
A -0.15709 ± 1.06661E-4
b 0.80766 ± 8.53025E-4
t 0.94248 ± 8.08514E-4
y0 0.24794 ± 2.61941E-5
x0 1.01 ± 0
Reduced Chi-Sqr 2.40378E-7
R-Square (COD) 0.99978
Adj. R-Square 0.99978

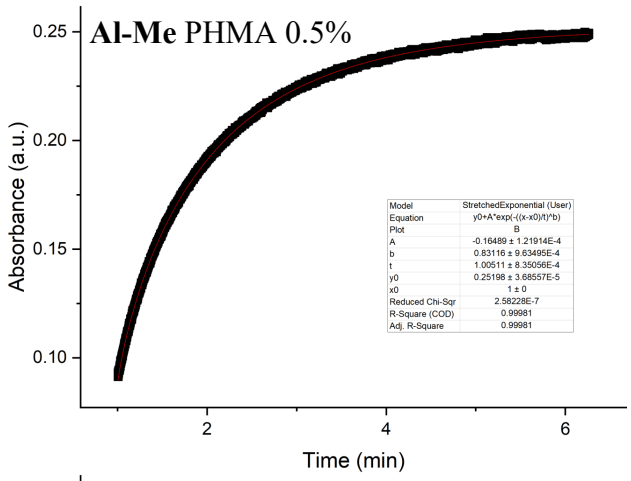
Al-Me PHMA 0.5%
Absorbance (a.u.)
Time (min)
Model StretchedExponential (User)
Equation y0+A*exp(-((x-x0)/t)^b)
Plot B
A -0.16489 ± 1.21914E-4
b 0.83116 ± 9.63495E-4
t 1.00511 ± 8.35056E-4
y0 0.25198 ± 3.68557E-5
x0 1 ± 0
Reduced Chi-Sqr 2.58228E-7
R-Square (COD) 0.99981
Adj. R-Square 0.99981

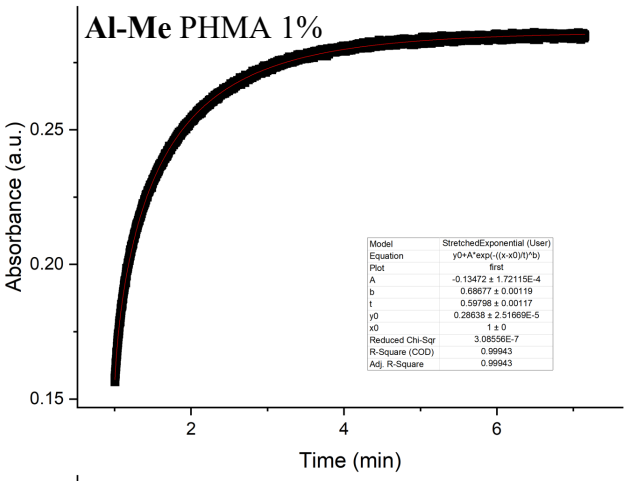
Al-Me PHMA 1%
Absorbance (a.u.)
Time (min)
Model StretchedExponential (User)
Equation y0+A*exp(-((x-x0)/t)^b)
Plot first
A -0.13472 ± 1.72115E-4
b 0.68677 ± 0.00119
t 0.59798 ± 0.00117
y0 0.28638 ± 2.51669E-5
x0 1 ± 0
Reduced Chi-Sqr 3.08556E-7
R-Square (COD) 0.99943
Adj. R-Square 0.99943

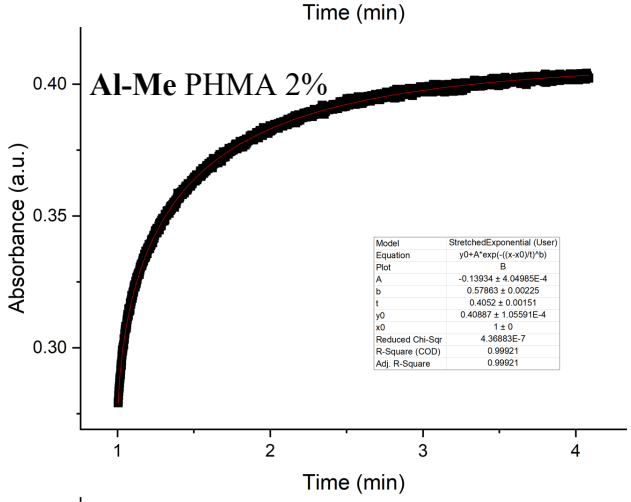
Al-Me PHMA 2%
Absorbance (a.u.)
Time (min)
Model StretchedExponential (User)
Equation y0+A*exp(-((x-x0)/t)^b)
Plot B
A -0.13934 ± 4.04985E-4
b 0.57863 ± 0.00225
t 0.4052 ± 0.00151
y0 0.40887 ± 1.05591E-4
x0 1 ± 0
Reduced Chi-Sqr 4.36883E-7
R-Square (COD) 0.99921
Adj. R-Square 0.99921

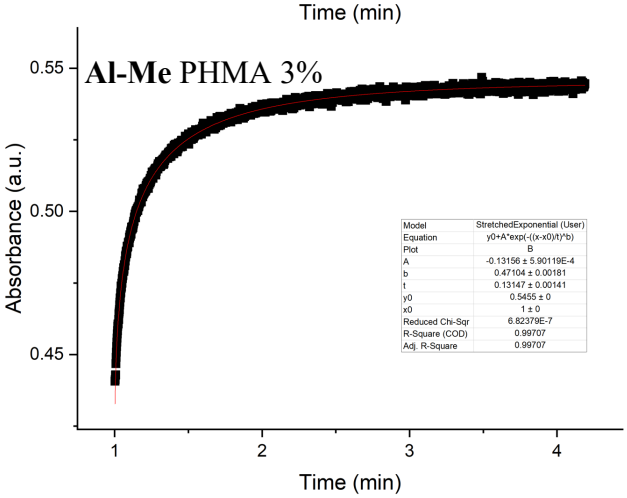
Al-Me PHMA 3%
Absorbance (a.u.)
Time (min)
Model StretchedExponential (User)
Equation y0+A*exp(-((x-x0)/t)^b)
Plot B
A -0.13156 ± 5.90119E-4
b 0.47104 ± 0.00181
t 0.13147 ± 0.00141
y0 0.5455 ± 0
x0 1 ± 0
Reduced Chi-Sqr 6.82379E-7
R-Square (COD) 0.99707
Adj. R-Square 0.99707

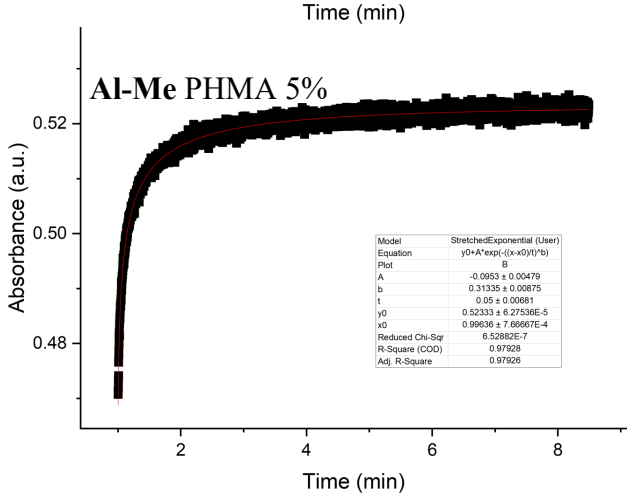
Al-Me PHMA 5%
Absorbance (a.u.)
Time (min)
Model StretchedExponential (User)
Equation y0+A*exp(-((x-x0)/t)^b)
Plot B
A -0.0953 ± 0.00479
b 0.31335 ± 0.00875
t 0.05 ± 0.00681
y0 0.52333 ± 6.27536E-5
x0 0.99636 ± 7.66667E-4
Reduced Chi-Sqr 6.52682E-7
R-Square (COD) 0.97928
Adj. R-Square 0.97926

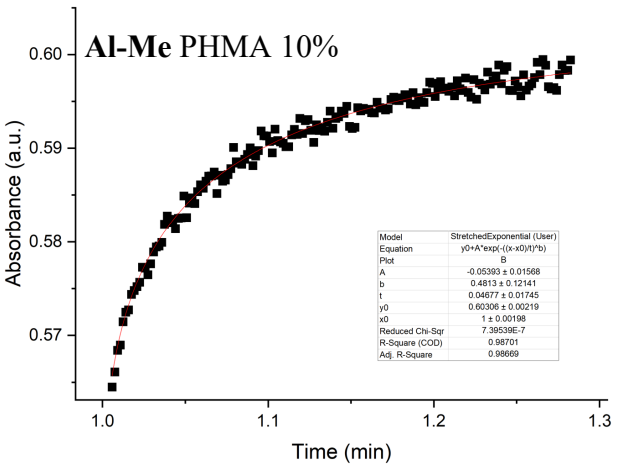
Al-Me PHMA 10%
Absorbance (a.u.)
Time (min)
Model StretchedExponential (User)
Equation y0+A*exp(-((x-x0)/t)^b)
Plot B
A -0.05393 ± 0.01568
b 0.4813 ± 0.12141
t 0.04677 ± 0.01745
y0 0.60306 ± 0.00219
x0 1 ± 0.00198
Reduced Chi-Sqr 7.39539E-7
R-Square (COD) 0.98701
Adj. R-Square 0.98669

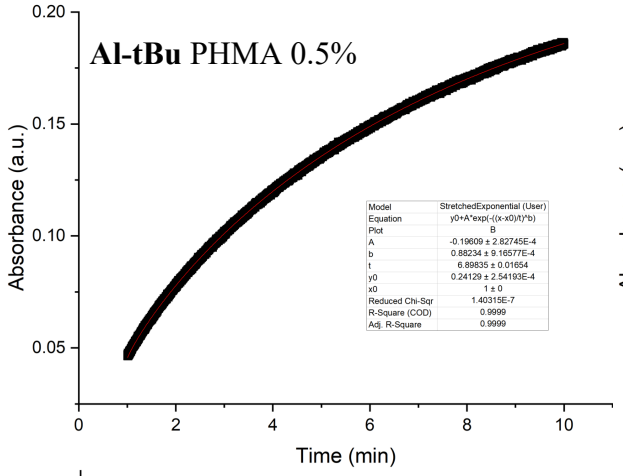
Al-tBu PHMA 0.5%
Absorbance (a.u.)
Time (min)
Model StretchedExponential (User)
Equation y0+A*exp(-((x-x0)/t)^b)
Plot B
A -0.19609 ± 2.82745E-4
b 0.88234 ± 9.16577E-4
t 6.89835 ± 0.01654
y0 0.24129 ± 2.54193E-4
x0 1 ± 0
Reduced Chi-Sqr 1.40315E-7
R-Square (COD) 0.9999
Adj. R-Square 0.9999

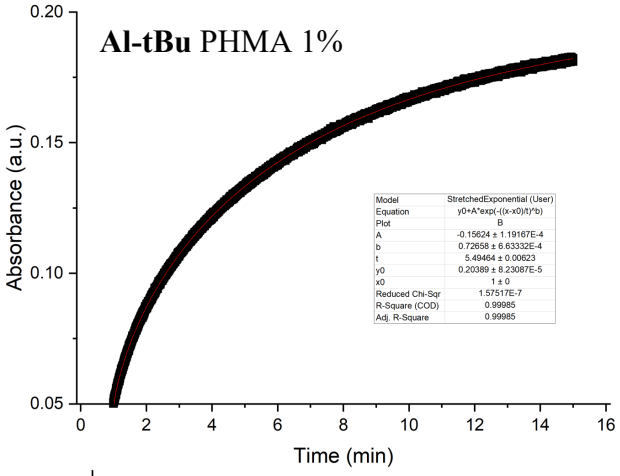
Al-tBu PHMA 1%
Absorbance (a.u.)
Time (min)
Model StretchedExponential (User)
Equation y0+A*exp(-((x-x0)/t)^b)
Plot B
A -0.15624 ± 1.19167E-4
b 0.72658 ± 6.63332E-4
t 5.49464 ± 0.00623
y0 0.20389 ± 8.23087E-5
x0 1 ± 0
Reduced Chi-Sqr 1.57517E-7
R-Square (COD) 0.99985
Adj. R-Square 0.99985

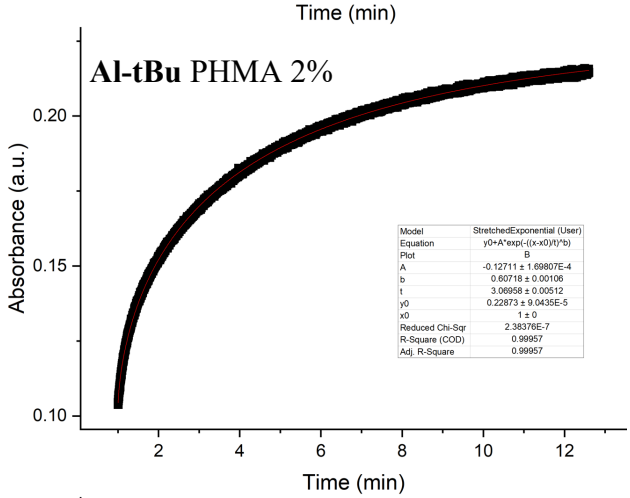
Al-tBu PHMA 2%
Absorbance (a.u.)
Time (min)
Model StretchedExponential (User)
Equation y0+A*exp(-((x-x0)/t)^b)
Plot B
A -0.12711 ± 1.69807E-4
b 0.60718 ± 0.00106
t 3.06958 ± 0.00512
y0 0.22873 ± 9.0435E-5
x0 1 ± 0
Reduced Chi-Sqr 2.38376E-7
R-Square (COD) 0.99957
Adj. R-Square 0.99957

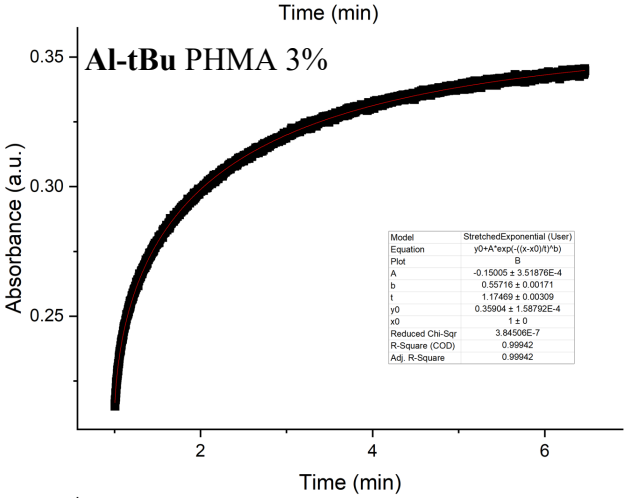
Al-tBu PHMA 3%
Absorbance (a.u.)
Time (min)
Model StretchedExponential (User)
Equation y0+A*exp(-((x-x0)/t)^b)
Plot B
A -0.15005 ± 3.51876E-4
b 0.55716 ± 0.00171
t 1.17469 ± 0.00309
y0 0.35904 ± 1.58792E-4
x0 1 ± 0
Reduced Chi-Sqr 3.84506E-7
R-Square (COD) 0.99942
Adj. R-Square 0.99942

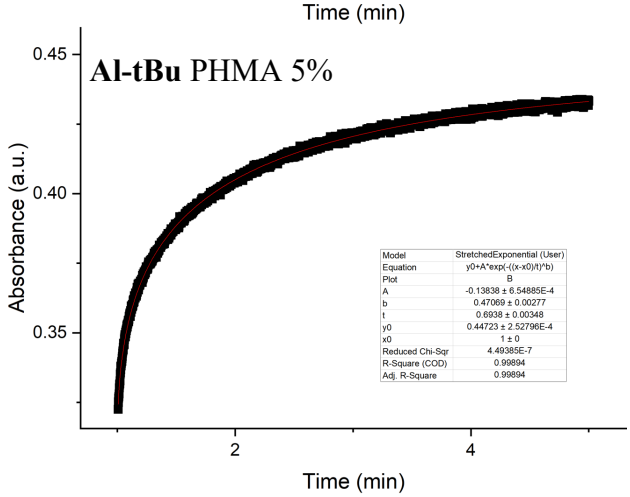
Al-tBu PHMA 5%
Absorbance (a.u.)
Time (min)
Model StretchedExponential (User)
Equation y0+A*exp(-((x-x0)/t)^b)
Plot B
A -0.13838 ± 6.54885E-4
b 0.47069 ± 0.00277
t 0.6938 ± 0.00348
y0 0.44723 ± 2.52796E-4
x0 1 ± 0
Reduced Chi-Sqr 4.49385E-7
R-Square (COD) 0.99894
Adj. R-Square 0.99894

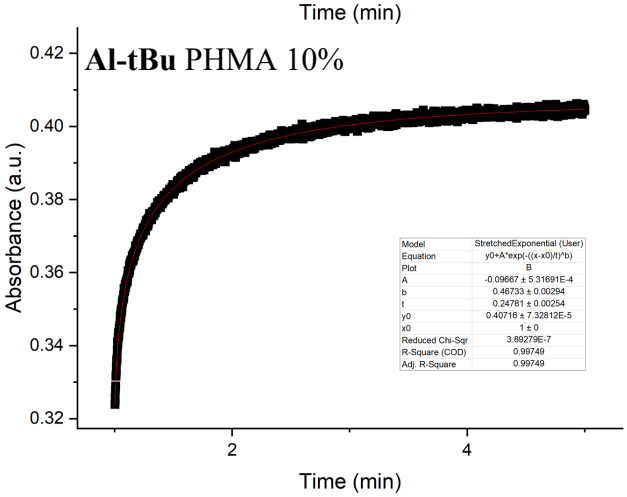
Al-tBu PHMA 10%
Absorbance (a.u.)
Time (min)
Model StretchedExponential (User)
Equation y0+A*exp(-((x-x0)/t)^b)
Plot B
A -0.09667 ± 5.31691E-4
b 0.46733 ± 0.00294
t 0.24781 ± 0.00254
y0 0.40716 ± 7.32812E-5
x0 1 ± 0
Reduced Chi-Sqr 3.89279E-7
R-Square (COD) 0.99749
Adj. R-Square 0.99749

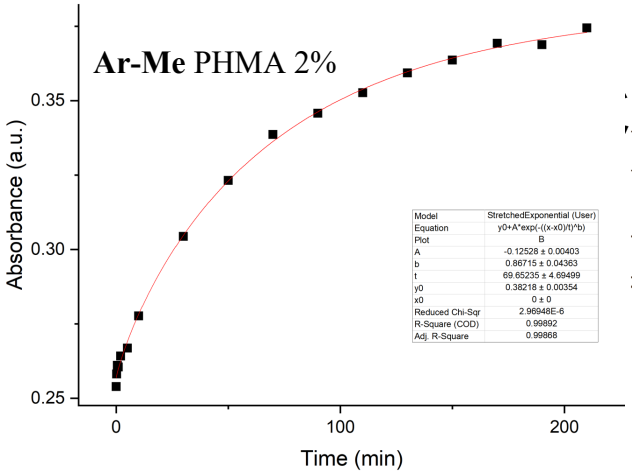
Ar-Me PHMA 2%
Absorbance (a.u.)
0.35
0.30
0.25
0
100
200
Time (min)
Model StretchedExponential (User)
Equation y0+A*exp(-((x-x0)/t)^b)
Plot B
A -0.12528 ± 0.00403
b 0.86715 ± 0.04363
t 69.65235 ± 4.69499
y0 0.38218 ± 0.00354
x0 0 ± 0
Reduced Chi-Sqr 2.96948E-6
R-Square (COD) 0.99892
Adj. R-Square 0.99868

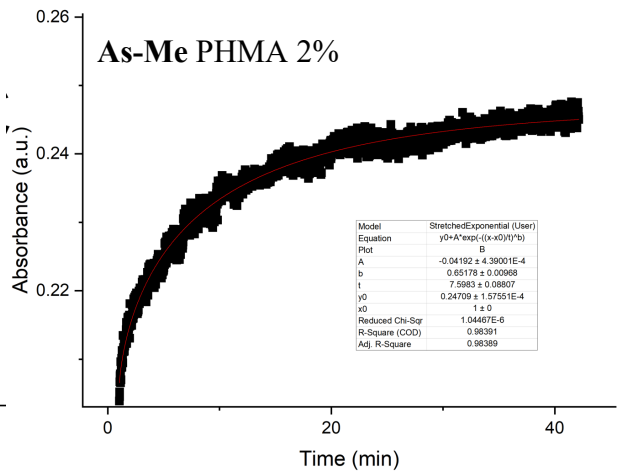
As-Me PHMA 2%
Absorbance (a.u.)
0.26
0.24
0.22
0
20
40
Time (min)
Model StretchedExponential (User)
Equation y0+A*exp(-((x-x0)/t)^b)
Plot B
A -0.04192 ± 4.39001E-4
b 0.65178 ± 0.00968
t 7.5983 ± 0.08807
y0 0.24709 ± 1.57551E-4
x0 1 ± 0
Reduced Chi-Sqr 1.04467E-6
R-Square (COD) 0.98391
Adj. R-Square 0.98389

Sample preparation

Microscope glass slides (25 x 20 mm) were sonicated in isopropanol and acetone and dried. Meanwhile, ca. 100 mg of a given polymer was dissolved in a suitable mixture of higher- and lower-boiling solvents (toluene + dichloromethane or cyclohexanone + dichloromethane, depending on the polymer). Solvent volumes were measured precisely based on the exact mass of the polymer to yield a solution with a desired polymer concentration, and the volume of the indigo stock was taken into account for the concentration calculations. When the polymer had dissolved completely, the indigo stock (in dichloromethane) was added and the mixture filtered through a PTFE filter with 0.2 µm pores. The filtered solution was spin coated (800 rpm for 3 seconds and then 500 rpm for 30 seconds) on the glass slide and then kept at 60 °C (in darkness) for 10 minutes to evaporate off any residual solvent. The exact conditions for the preparation of each polymer film are listed in **Table S4**. Sufficiently thick, smooth and uniform films were acquired in all cases.

Table S4*. Polymer film preparation conditions.*

Polymer	(mg/ml)	Indigo	(m%)	Solvents
PHMA	400	Al-Me	0.25	Cyclohexanone : dichloromethane 1:3
PHMA	400	Al-Me	0.5	Cyclohexanone : dichloromethane 1:3
PHMA	300	Al-Me	1	Cyclohexanone : dichloromethane 1:3
PHMA	200	Al-Me	2	Cyclohexanone : dichloromethane 1:3
PHMA	200	Al-Me	3	Cyclohexanone : dichloromethane 1:3
PHMA	150	Al-Me	5	Cyclohexanone : dichloromethane 1:3
PHMA	100	Al-Me	10	Cyclohexanone : dichloromethane 1:3
PHMA	400	Al-tBu	0.5	Cyclohexanone : dichloromethane 1:3
PHMA	300	Al-tBu	1	Cyclohexanone : dichloromethane 1:3
PHMA	200	Al-tBu	2	Cyclohexanone : dichloromethane 1:3
PHMA	200	Al-tBu	3	Cyclohexanone : dichloromethane 1:3
PHMA	150	Al-tBu	5	Cyclohexanone : dichloromethane 1:3
PHMA	100	Al-tBu	10	Cyclohexanone : dichloromethane 1:3
PHMA	400	Ar-Me	0.5	Cyclohexanone : dichloromethane 1:3
PHMA	300	Ar-Me	1	Cyclohexanone : dichloromethane 1:3
PHMA	200	Ar-Me	2	Cyclohexanone : dichloromethane 1:3
PHMA	400	As-Me	0.5	Cyclohexanone : dichloromethane 1:3
PHMA	300	As-Me	1	Cyclohexanone : dichloromethane 1:3
PHMA	200	As-Me	2	Cyclohexanone : dichloromethane 1:3
PBMA	400	Al-Me	0.5	Cyclohexanone : dichloromethane 1:3
PBMA	300	Al-Me	1	Cyclohexanone : dichloromethane 1:3
PBMA	200	Al-Me	2	Cyclohexanone : dichloromethane 1:3
PBMA	200	Al-Me	3	Cyclohexanone : dichloromethane 1:3
PMMA	200	Al-Me	2	Cyclohexanone : dichloromethane 1:3
PMMA	200	Ar-Me	2	Cyclohexanone : dichloromethane 1:3
PMMA	200	As-Me	2	Cyclohexanone : dichloromethane 1:3
PS	400	Al-Me	0.5	Toluene : dichloromethane 1:3
PS	300	Al-Me	1	Toluene : dichloromethane 1:3
PS	200	Al-Me	2	Toluene : dichloromethane 1:3
PS	200	Al-Me	3	Toluene : dichloromethane 1:3

References

[1] Huang, C.-Y.; Bonasera, A.; Hristov, L.; Garmshausen, Y.; Schmidt, B. M.; Jacquemin, D.; Hecht, S. N,N′-Disubstituted Indigos as Readily Available Red-Light Photoswitches with Tunable Thermal Half-Lives. *J. Am. Chem. Soc.* **2017**, *139* (42), 15205–15211. https://doi.org/10.1021/jacs.7b08726.

[2] Handa Masami, Mizuta Kenji, Hirai Kenji, Okamura Daigo, Gushikawa Toru 2015: Oxime derivative, method of producing the same and insecticide comprising the same as active ingredient. Patent JP2015000848A.